Temperature/end point monitoring and modelling of a batch freeze-drying process using an infrared camera

European Journal of Pharmaceutics and Biopharmaceutics [ISSN: 0939-6411], 158, 113-122

DOI: 10.1016/j.ejpb.2020.10.023

Temperature/end point monitoring and modelling of a batch freeze-drying process using an infrared camera

Maitê Harguindeguy[1], *Davide Fissore*

Dipartimento di Scienza Applicata e Tecnologia, Politecnico di Torino,

Corso Duca degli Abruzzi 24, 10129 Turin, Italy.

[1] Corresponding author:
tel: +39-011-0904695
fax: +39-011-0904699
email: maite.harguindeguy@polito.it

Abstract

Temperature monitoring and accurate drying end time determination are crucial for final product quality in vacuum freeze-drying of pharmaceuticals. Whether crystalline or amorphous solutes are used in the formulation, product temperature during ice sublimation should be kept below a threshold limit to avoid damage to the product structure. Hence, there is a need to continuously monitor product temperature throughout the process. Current monitoring tools, such as thermocouples and Pirani gauge pressure sensors, have several limitations such as affecting product dynamics or imprecise end point determination. In this work, a monitoring tool based on infrared (IR) thermography is used for batch freeze-drying processes. Batches using three different vial sizes, with up to 157 vials, were studied, allowing to extend and better describe the representativeness of IR thermography for this application. The detailed axial temperature profiles obtained through IR imaging allowed not only a comprehensive non-invasive temperature monitoring of the product, but also tracking of the sublimation interface. IR temperature measurements and primary drying end point determination were compared to standard methods and thus verified. Parameters important for freeze drying design space calculation, namely the global heat coefficient (K_v) and cake resistance to vapor flow (R_p), were also accurately estimated with the proposed method.

Keywords
Freeze-drying, infrared thermography, primary drying, axial temperature, sublimation interface tracking, model parameters, IR, monitoring.

List of symbols

A	fit parameter for R_p, s^{-1}
A_v	vial bottom area, m^2
B	fit parameter for R_p, m^{-1}
H	axial position of the sublimation interface, -
ΔH_s	heat of sublimation, J kg^{-1}
J_q	heat flux to the product, W m^{-2}
J_w	mass flux, kg $s^{-1}m^{-2}$
K_v	overall heat transfer coefficient, W $m^{-2}K^{-1}$
L_{dried}	dried cake length, m
Δm	mass change, kg
$p_{w,c}$	water vapor partial pressure in the drying chamber, Pa
$p_{w,i}$	ice vapor partial pressure at the sublimation interface, Pa
Pi/Ba	thermal conductivity and capacitance gauges pressure ratio, -
Q	heat received by the product, J
R_p	cake resistance to vapor flow, m s^{-1}
$R_{p,0}$	fit parameter for R_p, m s^{-1}
T_{atm}	atmosphere's temperature, K
T_b	vial bottom temperature, K
t_d	gravimetric test duration, s

T_i	temperature at the sublimation interface, K
T_{obj}	object's temperature, K
T_{refl}	reflected apparent temperature, K
T_{shelf}	shelf temperature, K

Greeks

ε	object's emissivity, -
σ	Stefan–Boltzmann constant, W $m^{-2}K^{-4}$
τ	atmosphere's transmittance, -

Introduction

Recently, the coronavirus pandemic has shed light on the importance of the pharmaceutical industry, which already held a high economic value before. Between 2019 to 2024, worldwide prescription drug sales are expected to reach 1.18 trillion US dollars. Biotech products are expected to have nearly a 50% share of the top 100 pharma products being sold, despite the challenges they pose [1]. The most pertinent challenge to the present study is the need for stabilization processes for these biopharmaceuticals [2]. Notably, this is often done by converting them from liquid solutions to stable, solid state, final products. This addresses their short shelf-life and reduces transportation costs by avoiding the need for cold chain storage [3]. However, many of these molecules require sophisticated drying methods to ensure their effectiveness. Freeze drying, a low temperature drying process, is perfectly suitable for such products [4].

The freeze-drying process is carried out in three steps: freezing, primary drying and secondary drying. During the primary drying stage, the frozen liquid is removed from the product by sublimation, leaving an increasing dried layer as drying advances into the vial [5]. During this step, accurate process temperature monitoring is crucial to ensure product quality. In fact, whether the nature of the solute used is crystalline or amorphous, product temperature during primary drying should be kept below a threshold limit to avoid damage to the dried cake structure. The rate of sublimation is another important point in process design because it has to be compatible with the condenser capacity to avoid choked flow in the duct between the drying chamber and condenser [6]. Finally, since the sublimation interface moves with drying and the position of this interface indicates primary drying progress and can thus be used to determine primary drying end time. Once primary drying is over, shelf temperature is increased to promote the desorption of bounded water, in a process known as secondary drying. Accurate determination of primary drying end time is critical for product stability: prematurely raising

the heating fluid temperature can cause ice melting, leading to product damage. On the other hand, if the secondary stage is delayed, it leads to an unnecessary increase in the duration of the process and its associated costs [4].

One of the targets indicated by the Guidance for Industry PAT (Process Analytical Technology) issued in 2004 [7] is that product quality no longer has to be tested on the final product, but it has to be built-in or achieved by design. It is thus essential to have reliable and representative sensors and methods in place for adequate process monitoring and control.

A large array of sensors for freeze-drying process monitoring are available and have been described in the literature [8]. Regarding primary drying end time determination, Pirani gauge, dew point sensor, tuneable diode laser (TDLAS) and cold plasma ionization are frequently used methods [9]. However, all of them present limitations such as large uncertainties on the final point determination or issues with calibration. Combining near infrared spectroscopy, plasma emission spectroscopy, and wireless temperature measurements was proposed as a robust solution [10]. The use of combined methods can offer a more robust approach, although they can be more expensive and complex to manage practically.

Regarding temperature measurement, thermocouples are generally used in lab scale. Resistance thermal detectors (RTDs) are most frequently used in industrial-scale freeze-dryers because they are more robust and can be sterilized [11]. Different methods, such as optical fiber sensors (OFSs) [12], temperature remote interrogation systems (TEMPRIS) [13] and thin-film thermocouples (TFTCs) [14] have also been proposed. However, in the case of invasive sensors such as thermocouples, TEMPRIS and RTDs, proper product representativeness can be jeopardized. The presence of the sensor inside the vial affects product dynamics, besides being destructive. Furthermore, product monitoring until the end of the primary drying stage is often impossible, as thermocouple temperature profiles may start unexpectedly increasing before the end point. Non-invasive sensors have their own set of limitations. For example, TFTCs are as

cumbersome to practically place in vials as common thermocouples. Additionally, this sensor is in direct contact with the vial, covering a large surface area of its wall. This affects heat radiation effects on that vial, thus compromising batch representativeness.

The set of optimal operating conditions for a given product is generally obtained through extensive experimental work and, unfortunately, sometimes simply by trial and error [15]. The correct understanding of the heat and mass transfer mechanisms during freeze-drying allows determining the optimal operating conditions with just a few runs. In-line process design is also possible if appropriate tools for product temperature and residual ice monitoring are available. These tools help characterizing the heat-flux from the shelf to the product and the mass flux from the sublimation interface to the chamber [16].

The use of an infrared thermal camera placed outside the freeze-dryer was proposed to monitor product temperature from above, without interfering with the product [17]. The use of an IR sensor was also proposed for continuous freeze-drying process monitoring [18]. However, the camera placement in both cases leaves room for improvement because the sensor can measure the whole product axial temperature if suitably positioned. To this end, an IR sensor placed inside the chamber was proposed by Lietta et al. [19] and its use investigated for small scale applications.

In this study, the IR sensor originally presented by Lietta et al. [19] is applied to larger freeze-drying batches, from 30 to 157 vials. Specifically, the goal of this paper is to:

(i) Evaluate if the presence of the IR sensor inside the chamber affects larger batch dynamics in any relevant way;

(ii) Verify temperature measurement accuracy compared to commonly used thermocouples. Additionally, check if less exposed frontline vials (with 5 neighbouring vials) in a hexagonal array can be used to represent central vial behaviour and thus, improve batch representativeness;

(iii) Check if the non-invasive IR temperature and sublimation interface position profiles allow a more precise primary drying end time determination by directly comparing them to the Pirani gauge method;

(iv) Use the IR measurements to estimate the parameters of a mathematical model, necessary to map out the design space of the primary drying stage through.

Materials & Methods

Freeze-dryer

Freeze-drying experiments were carried out in a REVO Freeze Dryer (Millrock Technology, Kingston, USA). This is is close to be completed. The onset and the offset of this decreasing interval can be used a pilot-scale freeze-dryer with roughly 1 m^2 of shelf area. It is provided with an external condenser with maximum condensing capacity of 30 kg operated at approximately -80 °C. It is also equipped with a thermocouple acquisition system in which T-type thermocouples (Tersid, Milano, Italy) were used. The freeze-dryer is also supplied with a thermal conductivity gauge (Pirani type PSG- 101-S, Inficon, Bad Ragaz, Switzerland) and a capacitance gauge (Baratron type 626 A, MKS Instruments, Andover, MA, USA) for pressure monitoring.

The ratio between the thermal conductivity and capacitance gauges signals (Pi/Ba) was used to assess a representative value for primary drying duration. The thermal conductivity gauge signal profile exhibits a sharp decreasing trend as the drying process to define the variability range of the drying time [9]. This is a broadly used method, although it presents wide variability ranges between the onset and offset times. This is physically correct since drying conditions, and thus drying duration, are non-uniform in the batch [20].

IR camera

The IR sensor system used (IMC Service S.r.l., Italy) in this study is the same sensor presented by Lietta et al. [19], specially designed for freeze drying applications. This system has a built-in thermal camera (FLIR Systems model A35; FLIR Systems Inc, Wilsonville, OR), a HDTV RGB camera (not used in this study), a processing board and an WiFi antenna for wireless data transfer. All components are mounted onto a polyacetal copolymer (Ertacetal C® natural) case, a thermal insulating, food grade, plastic material. For all tests, the IR sensor was placed inside the chamber, 25 cm away from the vials being monitored and on the same shelf. It was aligned with the shelf centreline, against the back wall.

An IR camera measures the temperature based on what *it sees*, which in this case is the glass wall on the outside of the vial. Van Bockstal et al. [18] proposed a 1D model to account for the temperature gradient between the external glass wall and the product to measure product temperature more accurately. However, the correction values tend to be small, a maximum 0.2°C adjustment was in fact found under similar conditions [21]. Because this is smaller than the accuracy of the IR sensor (+/- 1°C) and the thermocouple accuracy (+/- 1°C), this correction was not applied here.

In simplified terms, the IR sensor is a non-contact device that detects radiated infrared energy and converts it into an electronic signal, which is then processed to produce a thermal image. The emissivity of normal objects ranges from 0 to 1 [22]. The material emissivity depends on many parameters, such as the material type, the surface structure, the viewing angle between the camera and the object and the object temperature. The former three were always *the same* as they correspond to the glass vial. For the later, the behaviour and magnitude of the emissivity changes according to temperature on the material studied. In many applications, a constant emissivity value can be used. However, particularly when studying phase changes, care should be taken since the emissivity can change significantly which leads to errors in the measured values [22].

The software used in this study requires a single emissivity value to be fixed for the duration of the whole data acquisition session. Thus, a fixed emissivity value of 0.9 was used for the entire cycle. To fix this, IR temperature measurements were corrected using different emissivity values according to the estimated vial temperature range. This way, a value of 0.915 was used from 0°C to -10°C, 0.935 from -10°C to -20°C, 0.955 from -20°C to -33°C and 0.98 from -33°C to -40°C. These values were defined based on values reported by Colucci et al. [21]. To correct the measured values the total radiation (Q_{tot}) received by the sensor was calculated using **Equation (1)**:

$$Q_{tot} = \tau\varepsilon\sigma T_{obj}^4 + \tau(1 - \varepsilon)\sigma T_{refl}^4 + (1 - \tau)\sigma T_{atm}^4 \quad (1)$$

To this end, the parasitic radiation emitted from the environment towards the object can be regarded equivalent to the radiation of a fictitious body. This is accounted for as T_{refl}, the reflected apparent temperature of a *pure reflector* measured by the IR sensor. This *pure reflector* simply consists of a sheet of wrinkled aluminium foil according to the ISO 18434-1 2008 guideline, Part 1, Annex A [23]. Additionally, since chamber pressure is very low during drying (8 Pa in this study), the atmosphere's transmittance (τ) becomes near unity. Thus, the atmospheric influence in the final temperature measurement becomes very small, near 0.01°C in similar conditions [24], hence it can be neglected. This way, the corrected T_{obj} was calculated based on the adjusted emissivity values according to the temperature interval range.

Products and vials

The experiments were carried out using mannitol or sucrose (Sigma-Aldrich, purity ≥ 99.5%) solutes with ultra-pure water by a Millipore water system (Milli-Q RG, Millipore, Billerica, MA). Glass vials of sizes 4R, 6R and 20R (Schott Pharmaceutical Packaging, Inc., Lebanon, USA) were used, partially stoppered with an igloo stopper (NovaPure Chlorobutyl Igloo Stoppers, West Pharma, Exton, USA) after filling.

The 4R vials were processed with a 5% w/w mannitol solution, 6R with a 5% w/w sucrose and 20R with a 10% w/w sucrose solution. Amorphous solutes, such as sucrose, can present some cake collapse if the product temperature is not kept below the glass transition temperature [25]. Since the 4R has the largest surface area relative to the vial volume, due to proportionally larger heat radiation effects product temperature control during primary drying can be compromised, especially for edge vials. Thus, mannitol, as a crystalline solute, was chosen for this vial size to avoid collapse issues. Both types of solutes were used in this study since testing different possibilities makes the research more detailed.

The fill volumes used were respectively 1.5 mL, 3 mL, and 5 mL for 4R, 6R and 20R vials, thus resulting in a product thickness of approximately 12, 11 and 10 mm. The batch sizes were 157 vials (52 edge) for the 4R, 105 vials (39 edge) for 6R and 30 (12 edge) for 20R. The batches were directly loaded onto the shelf and arranged in a hexagonal array without tray sides.

Parameters calculation

To simulate in silico product dynamics throughout the process, 1D models can be used with good accuracy [26]. Assuming the heat flux (J_q) to be proportional to the temperature gradient between the shelf (T_{shelf}) and the vial bottom (T_b), **Equation (2)** can be derived, where K_v is the overall heat transfer coefficient.

$$J_q = K_v\left(T_{shelf} - T_b\right) \quad (2)$$

Assuming the water vapor mass flow (J_w) to be proportional to the water partial pressure difference between the sublimation interface ($p_{w,i}$) and the drying chamber ($p_{w,c}$), **Equation (3)** is obtained. The proportionality parameter R_p is the cake resistance to vapor flow.

$$J_w = \frac{1}{R_p}\left(p_{w,i} - p_{w,c}\right) \quad (3)$$

Equation (4) can be used to calculate $p_{w,i}$:

$$p_{w,i} = e^{(28.935 - \frac{6150}{Ti})} \quad (4)$$

while $p_{w,c}$ can be approximated to the chamber pressure, as the gas in the chamber is close to 100% water vapor. Finally, the energy balance at the sublimation interface is given by **Equation (5)** in which ΔH_s is the heat of sublimation [27]:

$$J_q = \Delta H_s J_w \quad (5)$$

Typically, K_v is estimated with a gravimetric test, as described in the literature [28–30]. For this, the total heat received (Q) by the product during a truncated ice sublimation session is assumed to be used for phase change from ice to vapor. The mass change (Δm) is computed weighting the vials before and after the sublimation session. This way, the mass-energy balance can be described as in **Equations (6)** and **(7)**:

$$Q = \Delta m \Delta H_s \quad (6)$$

$$Q = K_v A_v \int_0^{t_d} (T_{shelf} - T_b) dt \quad (7)$$

where A_v is the vial bottom area and t_d is the duration of the sublimation step. For the gravimetric tests carried out in this study, a digital scale set at four-decimal-point precision was used (Mettler Toledo, MS204S/01). Once the freezing step was completed, primary drying was carried out for approximately 3 hours to calculate K_v. Once K_v is known, J_q can be calculated using (**2**). Knowing J_q and ΔH_s, J_w can be calculated through **Equation (5)** and R_p can then be calculated using **Equation (3)**.

R_p has a dependence on the dried cake thickness (L_{dried}), which can be estimated through numerical integration of the water mass flux (J_w). To properly account for this dependence between R_p and L_{dried}, **Equation (9)** was frequently used, as seen in Bosca & Fissore [4].

$$R_p = R_{p,0} + \frac{AL_{dried}}{1 + BL_{dried}} \quad (9)$$

In this model, $R_{p,0}$, A and B are fitted experimentally based on the R_p and L_{dried} values calculated using **Equations (3)** and **(4)**.

Experimental design

Based on this study objectives, the experiments were divided into three groups to assess: (i) potential effects of the sensor inside the chamber, (ii) sensor's accuracy for temperature measurement and (iii) accuracy for end time determination. The fourth study objective, (iv) model parameter estimation, was based on the temperature profiles obtained in the second and third groups of experiments.

All experiments used the same operating conditions to reduce the number of independent variables and enable direct comparisons. Thus, only the vial diameter, batch size and solution were varied between the groups. The presence or absence of the IR sensor inside the chamber in each batch depended on the experimental design. All batches had at least 2 thermocouples placed in edge vials and 2 in central vials for conventional process monitoring.

Freezing lasted 2 hours, with a 1 h freezing ramp from 20°C to -40°C (1°C/min) and then 1 h hold at -40°C. Primary drying was done at -20°C shelf temperature and 8 Pa chamber pressure. The complete freeze-drying tests were done until the Pi/Ba signal reached the offset time, plus a couple extra hours to ensure primary drying was over. For the gravimetric tests, different durations were done for each vial size tested. Still, care was taken to ensure the same primary drying duration for each given vial size, in order to enable direct comparisons. This way, the gravimetric tests lasted 250 minutes for 4R, 260 minutes for 6R and 180 minutes for 20R vial sizes.

(i) Evaluation of the sensor's effect inside the drying chamber

To evaluate if the IR sensor presence inside the chamber affects the batch dynamics in any way, gravimetric and complete freeze-drying tests were carried out. Each test was done with and without the IR sensor inside the chamber. To reduce the independent variables for this group of

experiments, all temperature comparisons are based solely on thermocouple measurements. Mass change in the vials, temperature profiles, values of K_v, and batch duration, for the complete tests, were compared between the tests, with and without the IR sensor presence.

It is known that according to the vial position in a batch, it will be exposed differently to the heat radiation from the walls [31]. Additionally, the temperature difference between walls and the vial will directly contribute to the radiated heat from the walls. This means that if the walls are relatively cooler, they would have less of a contribution to the heat radiated to the vials. Since the camera was placed against the back wall, it was shielding the vials from part of the back-wall radiation, while exposing them to the heat being radiated from the sensor case itself. Whether the camera plays a radiating or shielding effect depends on the relative temperature behavior of the case and the wall. Thus, one extra gravimetric experiment was done for 6R vials only, using the same 1 h freezing ramp, but then holding the product at -40°C for 5 h. This was done to briefly explore if freezing duration had any impact on the IR sensor's radiating or shielding nature. Thermocouples were placed on the back wall and on the sensor's case to evaluate their temperature and better understand their radiating or shielding effects on the batch.

(ii) Sensor accuracy for batch temperature monitoring

An important limitation of IR imaging is the inability to measure the temperature profiles of vials out of the sensor's field of view. Thus, only front row vials can be monitored, and these are the vials where the temperature of the product is higher due to radiation effects. Additionally, ice sublimation is completed earlier in those vials than in centre ones. It is therefore of interest to find a solution to monitor central vials.

As presented by [31], vial temperature and sublimation interface profiles are slightly different for each type of vial according to its position in an hexagonal array. From their results,

vials in a more shielded position, such as the hatched ones in **Figure 1**, present a closer behaviour to central vials, although they are still different. In this study, the use of a hexagonal array as a mean to achieve better batch representativeness is evaluated.

Throughout the text, the IR temperature measurements of fully exposed vials are called *~edge*, while those of the less exposed ones are called *~central*. They will be considered equivalent to edge and central vials monitored by thermocouples in all comparisons between both sensors. It should be noted that this approximation to extrapolate central vial temperature profiles by the IR sensor was applied only for IR data extraction. All thermocouple average temperature profiles and K_v calculations regard vials with less than 6 neighbouring vials as edge vials.

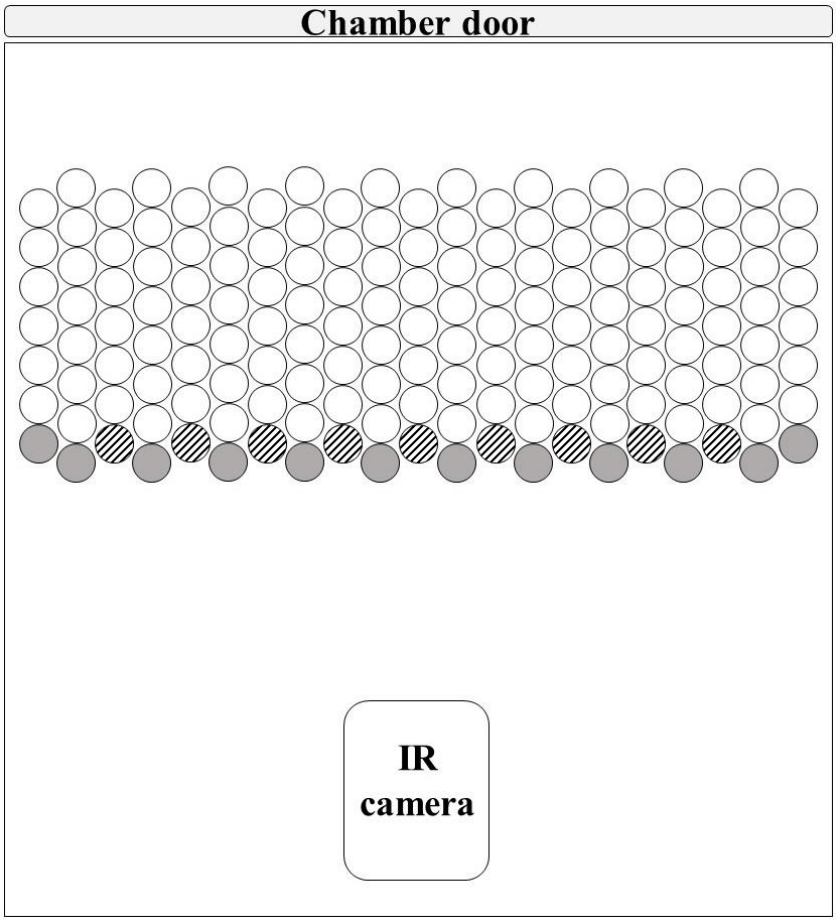

Figure 1. Illustration of the hexagonal array used in this study. The grey solid filled vials were considered representative of edge vials (~edge) while the hatched vials were considered representative of central vials (~central).

The average IR bottom temperature was compared to the thermocouple values. This average was calculated based on the temperature values from six equally spaced pixels positioned on the bottom of the vial. Data noise typically present in IR thermal imaging has been be reduced with this averaging.

IR *~edge* and *~central* average temperatures were compared to edge and central thermocouple measurements from the same batch. Additionally, the K_v and R_p values, calculated from the temperature measurements were compared. The proper and accurate estimation of these parameters by the IR camera is crucial to verify the sensor application for process cycle design and optimization.

(iii) IR sensor-based primary drying end time estimation

One of the great advantages of using thermal imaging is the ability to obtain the whole axial temperature profiles. From this, several pieces of information can be extracted. During primary drying, since sublimation is an endothermic process, the product sublimation interface presents a lower temperature compared to the rest of the product. This interface moves down the vial during primary drying, as the L_{dried} increases, until all the frozen water is removed. The interface position can be located and tracked as the pixel with the local temperature minima during drying.

In this group of experiments, six axial temperature profiles were extracted for each vial, i.e. six vertical lines of pixels equally spaced across each vial. For each line, the pixel with the minimum temperature was located, which was regarded as the line interface temperature (T_i). By extracting the mean T_i value from those six lines, the vial T_i profile was traced. For the interface position tracking (H), since a unidimensional approach is considered, an average of the T_i pixel position from the six lines was calculated. This can be seen represented in **Figure 2**.

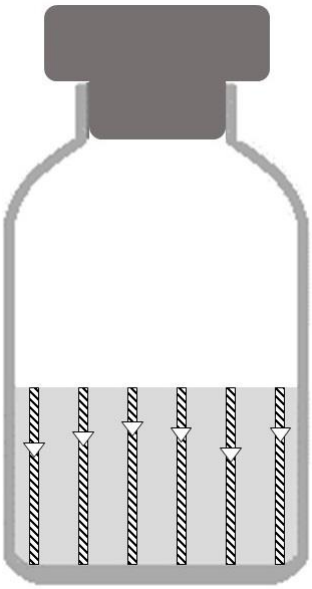

Figure 2. Graphical scheme of the data acquisition lines and sublimation interface positions for an arbitrary timeframe. Hatched vertical columns represent the acquisition lines used; the white triangles represent the sublimation interface position, tracked as the local minimum temperature in each acquisition line.

Two IR based alternative methods to determine primary drying end-time were investigated. The first was based on tracking the position of the sublimation interface, H, as it should reach the bottom of the vial once primary drying is over. The second was based on the measurement of T_i, noting that when this temperature begins to increase, primary drying is over. The widespread Pi/Ba method was used to give a reference end-time and, thus, evaluate the accuracy of the T_i and H based methods proposed. Additionally, as a more direct estimation for comparisons, the end-time based on the average batch K_v value was also used. This method consists of estimating the necessary drying time to sublimate all water present using **Equations (6)** and **(7)**.

To compare each method in a more objective way, a custom MATLAB (MATLAB R2019b © 1994-2020 The MathWorks, Inc) code was developed. A curve was fitted to the data to allow the use of derivatives to infer inflection points of interest in an automated way. The

inflection point of interest for T_i is the ascending interval after a few hours of primary drying. For the Pi/Ba curve, the inflection point of interest is the descending trend, after a few hours of drying. The fitting used for T_i and Pi/Ba was a non-parametric smoothing spline, which fits a set of intersecting polynomials to the data. The function is controlled by a smoothing parameter which, the larger it is, it makes the fit smoother. The fit was calculated using MATLAB built-in *smoothingspline* function with the default parameter set, which optimizes the smoothing parameter automatically [32].

Based on the curve fitting, the points of interest were identified, and the end time estimate from each method was computed for further comparison. For the T_i and Pi/Ba curves, the maximum and minimum values for the first derivate of the fitted curve were defined as the inflection points of interest, respectively. Based on each inflection point, a tangent line was built. This tangent line had its slope calculated using the average inclination of the signal curve (T_i or Pi/Ba). This was based on a 2 hour-time-interval, immediately before and after the inflection point. The use of a tangent in an inflection point to identify points of interest in a data curve is a simple and commonly used method [33]. The difference in this study was simply to apply it in a standardized way, to compare the values more objectively.

Thus, the intercept between this tangent and the upper temperature plateau, defined the T_i end-time. While the interception point between this tangent and the upper and lower pressure ratio plateaux, defined the Pi/Ba onset and offset end-times.

The point of interest for H, is the zero-crossing, indicating that all the ice sublimated, and primary drying is over. However, due to the resolution of the IR image, the last pixel tracking this profile was not a clear indicator of the exact end point. Still, the end time interval could be easily observed as the minimum span after a few hours of primary drying. To automate the endpoint determination, the best H profile fit was an exponential function. This, of course, prevented the use of derivates or having the function reach zero to identify the endpoint. Thus,

this was defined by an empirical threshold value of 0.005 that worked properly for all vial sizes and permitted the automation of the primary endpoint detection task.

Statistical analysis

The comparisons done always confronted mean values from two groups at a time. This way, analysed values were first tested to verify if they followed a normal distribution and then they were compared using a Student's t-test [34]. The t-tests done were two tailed, two-sample (independent) t-tests assuming an unknown variance and considering a 95% confidence interval.

Results & Discussion

Based on the objectives of this study, the results discussed will be divided into four subsections: (i) the assessment of the potential sensor's effect, (ii) temperature monitoring, (iii) primary drying end-time estimation and (iv) model parameters estimation.

(i) Investigation of the sensor effect on monitored batches

As described in the Materials & Methods section, since this sensor is placed inside the drying chamber a series of tests were performed to understand if its presence can affect the batch dynamics in any way. The current study applies a sensor as proposed by Lietta et al. [16] for a larger set of vials (157) positioned in a hexagonal array.

No differences in mass change were observed for all tested vial sizes ($p>0.05$) after the gravimetric tests (graphical results in the appendix, **Figure A.1**). Loss of mass was higher for edge vials compared to central vials and first-row vials, facing the sensor, were comparable to edge vials.

The temperature profiles for 4R vials in both gravimetric tests, with and without the

sensor, are presented in **Figure 3**. From these results, the temperature profiles seem similar although the test with the sensor presented lower temperatures with differences of up to 1.2% for central vials and 4.0% for edge vials. This is reflected on the first-row mass change for this test which was 6.5% lower compared to the test done without the sensor. This could indicate a small shielding effect as reported before by Lietta et al. [19]. However, results varied for the other vials tested. 6R temperature profiles (**Figure A.3 A**) with the sensor were up to 2.2% lower for central vials while up to 1.2% higher for edge vials. 20R temperatures (**Figure A.3 B**) were up to 1.5% lower for edge and central profiles. Further checking first row mass change for 6R and 20R vials, they had +5.8% and -1.4% difference compared to the tests without the sensor, which agrees to the temperature profile differences observed. Nonetheless, these variations were regarded as small indicating little, if any, relevant effect from the sensor's presence inside the chamber.

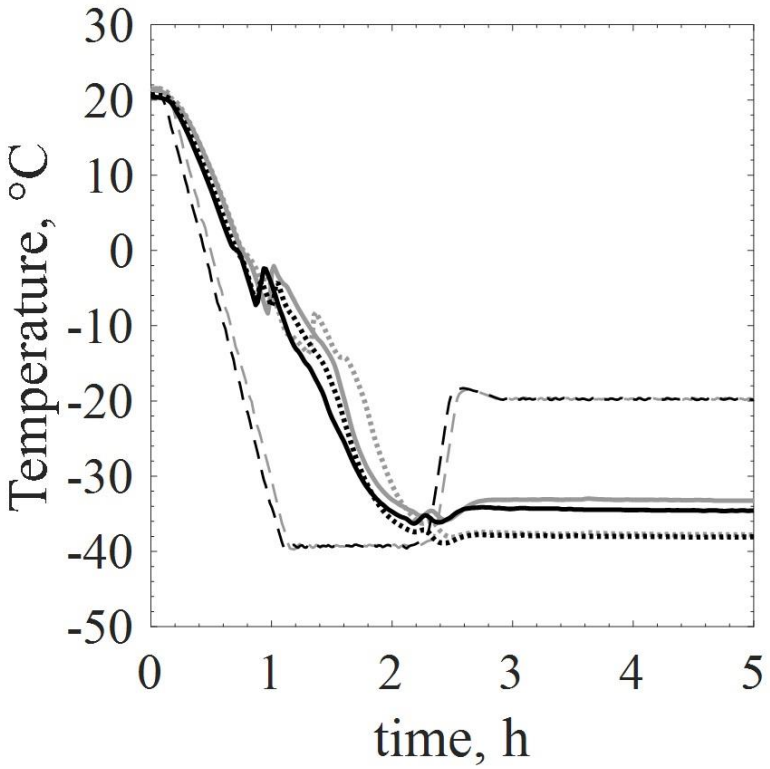

Figure 3. Temperature profiles during the gravimetric tests for 4R vials. Gray lines represent the test without the IR sensor while black lines represent the test with the IR sensor. Continuous lines (-) are used for edge vials, dotted lines (.) are used for central vials while dashed lines (- -) are used for the shelf temperature throughout the test.

As described in the Materials & Methods section, an extra test was performed using the 6R vials, using a 6-hours freezing duration instead of 2 hours. In this experiment, in contrast with the test using a 2-hours freezing step, some shielding effect was observed from the resulting mass changes (**Figure A.2**), especially for the first row. At the end of long freezing, the sensor case front temperature was -20.4°C while the back-wall temperature was -12.1°C. At the end of the gravimetric test, their temperatures were -8.6°C and 2.4°C, respectively. This means there is roughly a 10°C difference between the sensor case and the back wall throughout the whole test. On the other hand, at the end of short freezing stage their temperatures were respectively -4.6 and -0.4°C for the sensor and back-wall, whereas at the end of the gravimetric test they were -3.3°C and 5.3°C. Since the sensor was in direct contact with the shelf, it makes sense that its temperature was lower than the back wall. When this difference between the sensor and wall temperature was small, shielding effects seemed negligible. When this difference was big enough, the cooler sensor seemed to have had a shielding effect. Thus, when long freezing is used, since the sensor temperature is relatively lower compared to the short freezing test, it could play a shielding role during freeze-drying, as reported before by Lietta et al. [19]. However, in shorter freezing conditions, such as the ones used in this group of experiments, this shielding effect becomes negligible.

Since K_v derives from mass change and temperature profiles, expectedly, the calculated values were similar between tests with and without the IR sensor (**Figure A.4**). For 6R and 20R batches there was no difference ($p>0.05$) while for 4R there was ($p<0.05$). Since the precision of all used instruments is the same for all tests, while 4R vials are much smaller with a larger batch size, it makes sense that small errors from the precision could result in more variations within and between tests.

Taking into account the non-uniform distribution of K_v values in a batch, it is necessary to investigate the distribution of K_v across the vials. A thermocouple-based K_v map for 4R vials

is shown in **Figure 4**. The central vials K_v values for the test without the IR sensor look a bit less homogeneous than the values in the test with it. Taking a deeper look, the K_v standard deviation is derived from the mass change standard deviation, which was about the same for both tests. More specifically, the initial mass standard deviations were 0.0784 and 0.0973 g (before the gravimetric test was done) and then 0.1180 and 0.1206 g after the gravimetric tests, respectively with and without the sensor. Hence, this was considered to not affect the comparisons in any significant way and the sensor's effect observing the K_v map was regarded as irrelevant. Results for 6R and 20R vials (**Figure A.5** and **Figure A.6** respectively) presented almost no change between tests.

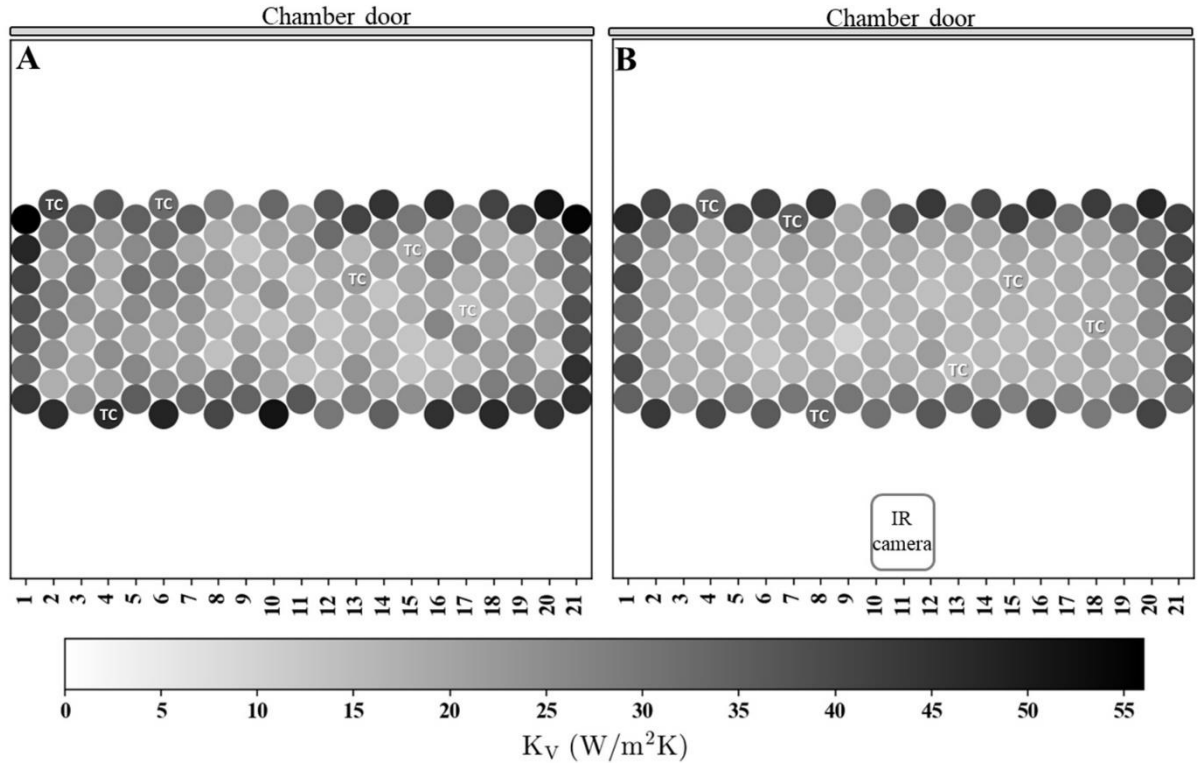

Figure 4. K_v map for 4R vials. A) Batch without the IR sensor inside the chamber; B) batch with the IR sensor inside the chamber.

Finally, the last aspect to be analysed was the effect of the presence of the sensor for a complete cycle and its duration. No relevant effect was observed in batch duration as identified

through the pressure ratio and temperature profiles for 4R an 6R vials (**Figure A.7 A** & **B**). However, for the 20R vials (**Figure A.7 C**) in the presence of the sensor, batch duration was approximately 3 h shorter and temperature values were slightly higher, in the order of 2°C, as observed in the gravimetric test for 20R vials (**Figure A.3 B**). These tests were repeated since they presented such a different result from what was previously observed for 4R and 6R. Still, the repeated test yielded the same result. A possible explanation could be an intensified heat radiating effect in the presence of the sensor since this was a small batch with 73% edge vials.

(ii) Temperature monitoring

Once it was clear that the sensor presence inside the chamber has minimal effects, it was important to verify the sensor capabilities in batch monitoring. To better understand the acquired IR temperature measurements, **Figure 5** displays the average bottom temperature measured per vial. The first point to be noted is the consistently lower temperature measured for the ~*central* vials compared to the ~*edge* ones, derived from the hexagonal array used. This is the first indicator that the hexagonal array approach may in fact help improve batch representativeness.

It is important to remark that the angle between the object of interest and the IR sensor can influence temperature accuracy. This means that vials away from the boresight of the camera, i.e. towards side edges, can have lower temperature estimation accuracy. Since the camera was placed in a centred position relative to the shelf and the vials, angle effects should equally affect leftmost and rightmost vials. In **Figure 5**, vial #1 (leftmost) seems to have the highest temperature, which at first might seem an accuracy problem. However, in the other batches, using 6R and 20R vials, this behaviour of the leftmost vial being warmer was also observed (**Figure A.8 A** and **A.8 B** respectively). Relatively to the camera field of view, the electric panels of the freeze dryer used were on the left side. Additionally, from the K_v map in

Figure 4 it can be inferred that the left side tends to be marginally warmer than the right side of the chamber, which could explain this behaviour. Still, this shows another great advantage of IR imaging: it easily allows the investigation and understanding of the heat distribution inside the equipment which in turn enables better process control and design.

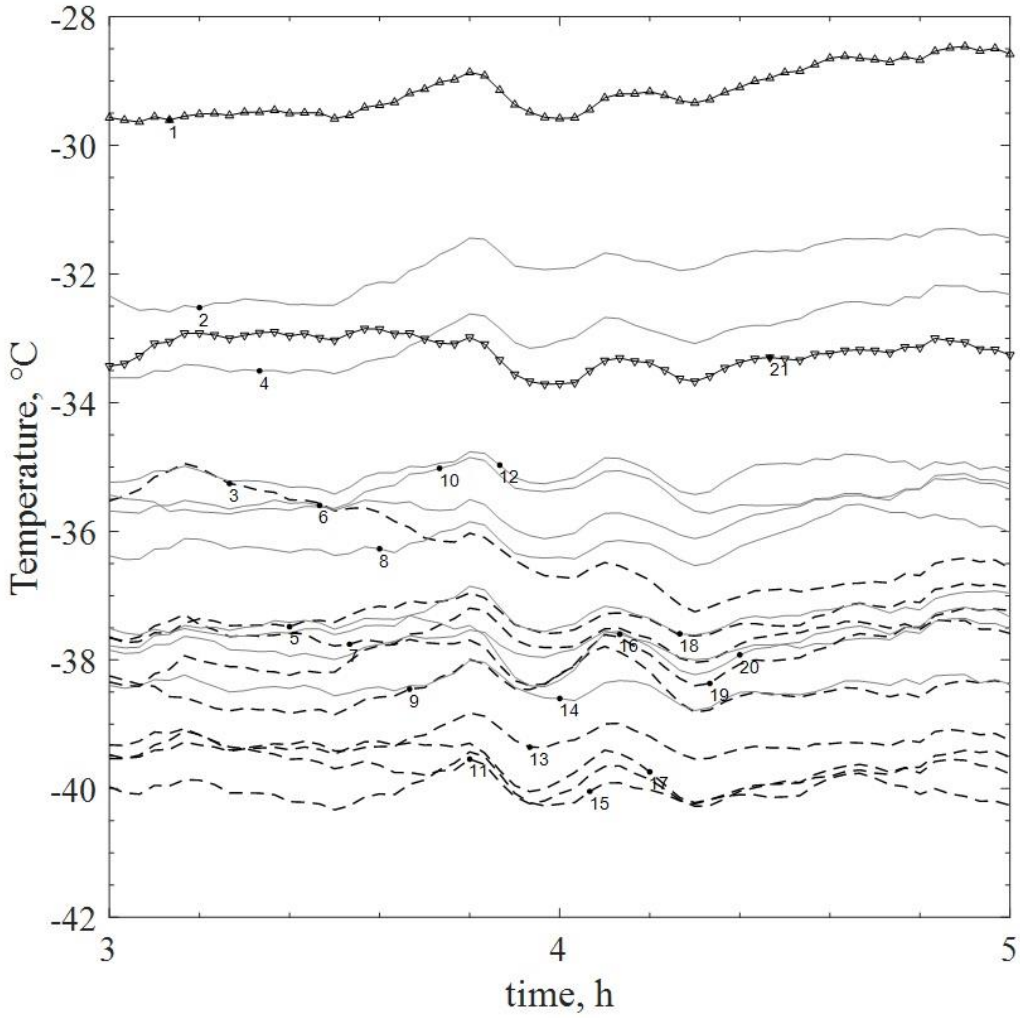

Figure 5. 4R IR bottom temperature profile per vial, in order from left to right, according to the thermal camera field of view. The first (leftmost) vial is represented with a line and triangle (-▲), the last (rightmost) vial is represented by a line and inverted triangle (-▼). For all other vials, dashed lines represent *~central* vials while continuous lines represent *~edge* vials. Graph zoomed for the last 2 hours of primary drying.

IR imaging provided a full and detailed portrait of the temperature per vial in the first row. Although these profiles seem widely distributed, with up to a 24% variation between *~edge*

vials and 12.2% between ~*central* ones, the average values are the practical ones for comparison with thermocouple measurements. **Figure 6** presents the average temperature measurements by thermocouples compared to the IR-derived temperatures from the same batch.

The IR sensor used in this study has a reliable accuracy until around -40°C. In the lowest point of freezing, it can be observed that it loses some of its accuracy, recording overall lower temperatures with a difference of up to 9°C in this section stretch compared to the thermocouple values. This trend was also observed for 6R and 20R vials batches (**Figure A.9 A** and **A.9 B**, respectively). Notwithstanding this fact, ~*central* average temperature was close to the thermocouple central average temperature profile during primary drying, within the sensors' accuracy of ±1°C. The ~*edge* average on the other hand was a bit off in the first hour of primary drying reaching up to a 8.5% difference, but after that it was within the thermocouple uncertainty range (±1°C), presenting approximately 2% difference in the measurement. For 6R and 20R, ~*edge* and ~*central* profiles were within the ±1°C uncertainty range most of the time, except for the 20R ~*edge* temperature in the last hour of primary drying, when it was higher than thermocouple measurements by nearly 1.5°C representing a 6.2% difference from thermocouple measurement.

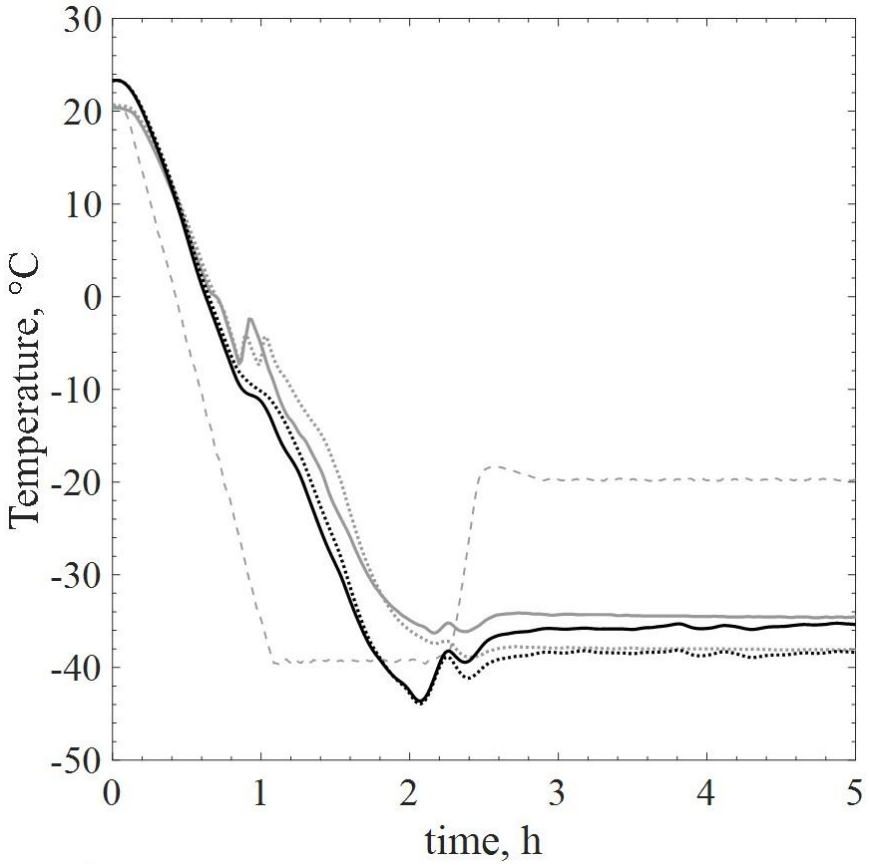

Figure 6. TC versus IR average bottom temperature profiles for the same 4R vial batch. Continuous black line (-), IR *~edge* vials. Dotted black line (.), IR *~central* vials. Continuous grey line (-), TC edge vials. Dotted grey line (.), TC central vials. Dashed grey line (- -), shelf temperature.

(iii) Primary drying end-time estimation

Because freeze drying is a long and energy-consuming process, optimization of any given stage is always desirable. The determination of primary drying end time is among the factors that can help save energy, time and, therefore, improve the overall cycle efficiency [35]. The end time can be inferred by many methods as mentioned in the Introduction. However, all methods have their limitations, leaving room for the development and introduction of new ones.

A widespread method is using the Pi/Ba as described in Materials & Methods. Since Pi/Ba signal onset and offset times tend to have a large uncertainty range, it is crucial to evaluate product temperature as well when trying to determine primary end time. This is helpful because when the sublimation is over, product temperature rises, which can be used to help

inferring the end of primary drying. However, the most used temperature measurement method, thermocouples, presents some issues. First, they are in direct contact with the product, affecting its dynamics and putting in doubt their representativeness of the whole batch. Second, unless the process is conducted by a well-trained operator, thermocouple misplacements are done, resulting in inaccurate temperature measurements [11]. Finally, even when a trained operator places the thermocouples properly, they may move during the process or the cake may break in such a way that it is not anymore representative of the batch. IR thermography, as a non-invasive method, does not pose these limitations and its temperature monitoring may be used alone to determine primary drying end-time.

Additionally, the H profile, i.e., the axial position profile of the sublimation interface, is investigated as a method to identify primary drying end. **Figure 7** shows the H, T_i and Pi/Ba profiles for a 4R vials batch, exhibiting the raw data (grey lines) as well as the fitted curves (black lines).

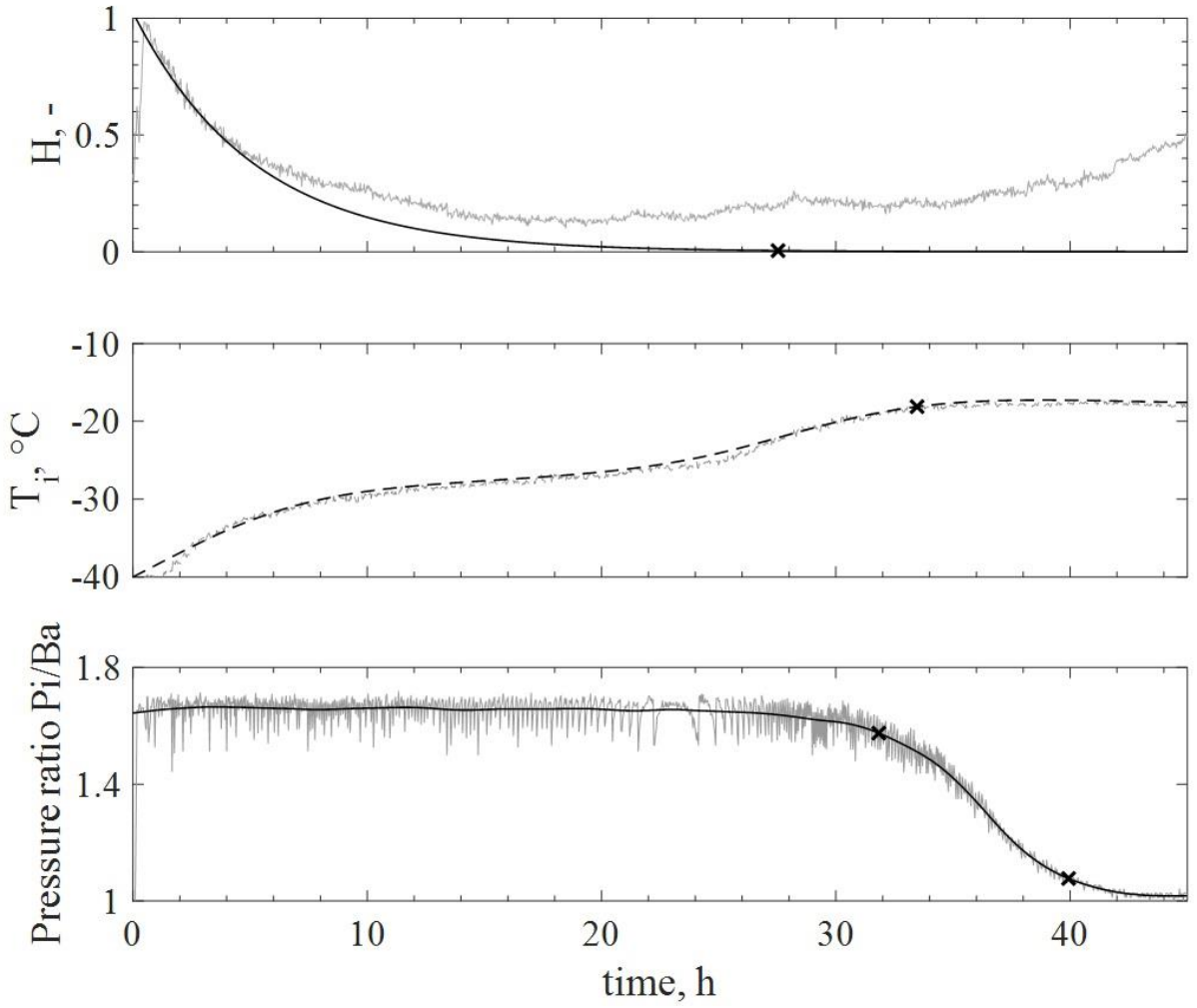

Figure 7. Different signals to identify primary end-time for 4R vials batch. The "x" markers indicate potential end-time points for primary drying for each signal. In A, B and C, grey lines represent the raw data while back lines represent the fitted curves. A) Adimensional *H* axial profile where 1 represents the top of the vial and 0 the bottom, B) $\boldsymbol{Ti}$ average profile, C) *Pi*/*Ba* profile.

The *H* profile has a particular behavior: it starts decreasing, but then, when it reaches the bottom, it becomes noisy and then it goes up. This happens because the IR camera resolution has a limited number of pixels and, when *H* reaches the last pixel on the bottom, tracking resolution is compromised. For the 4R vials fill volume, the cake profile had nearly 11 pixels, roughly 1 pixel per cake millimetre under the tested conditions.

In **Figure 7 A**, it can be observed that the *H* profile reaches a minimum value of 0.1014 at around 20 h and then it remains between this minimum and about 0.4. This behavior was also observed in the 6R and 20R vial batches (**Figure A.10** and **A.11**), this trend is an indicator that

primary drying is over. This happens since after sublimation is over, the product's temperature increases using the heat supplied by the shelf, moving the minimum temperature point up at this point in the process. When this is observed, it can be used to determine a representative point for primary drying end time. However, this way to identify the ending point would pose the same limitations as the Pi/Ba method as it would be a subjective determination. To overcome that, the end-time determination was based on a threshold value, as described in the Materials & Methods section. Accordingly, the chosen threshold value does match the region of increasing *H* profile position. That means, the same region that was used to determine the end time, indicating that this method can work as a more standardized one for this application. The estimated end-times based on all methods tested are listed in **Table 1**.

Table 1. Estimated primary drying end-times in hours (h), based on different signal indicators.

	H	T_i ~*edge*	T_i average	T_i ~*central*	Pi/Ba onset	Pi/Ba offset	K_v
4R	27.5	32.6	33.5	34.2	31.8	39.9	31.5
6R	20.9	24.1	26.1	27.4	25.6	33.1	24.9
20R	14.8	18.9	19.7	20.7	15.6	21.5	24.7

It is important to discuss *what* the thermal camera is measuring. As described in Material & Methods, the IR measurement is based on the glass vial wall, which is representative of the product inside. The unidirectional approach to interpret the moving interface works well for most of the cake length. However, as it reaches the bottom, it is not as flat anymore, particularly in case of large section vials, e.g. 20R. This way, the marginal profiles measured by the camera represent the external cake layer very well, but they cannot accurately represent the last, lower inner core of the frozen product. According to this, *H* estimated end-times could be slightly underestimated for larger vials, such as 20R. In fact, that seems to be the case in the results

obtained in this study. When comparing H and K_v end-time estimated values, the H durations were always smaller than the K_v based ones and the difference increased with vial size. Using the K_v estimated duration as a reference, these differences were 12.7% for 4R, 16.1% for 6R and 40.0% for 20R. Analogously, the Pi/Ba *onset* estimated end-time, also tends to be shorter and a possible indicator of primary drying end for edge vials. Comparing to the Pi/Ba onset values, the H estimated values diverged 13.6%, 18.4% and 5.1% for 4R, 6R and 20R, respectively.

On the other hand, even if there are temperature gradients in the vial, they are small enough so that T_i measurements were still representative of the vial temperature. This is reflected in the end-time estimation since it may be as accurate as it gets using a temperature-based method. Comparing T_i *average* end-time estimates, they seem to lay between Pi/Ba *onset and offset* times (**Figure 7)** and to be very close to the K_v estimates (except for the 20R vial).

There is always a big concern regarding the central vials, since they require longer drying times. To ensure complete primary drying of central vials, the Pi/Ba *offset* signal if often used, as it would represent a more conservative approach to ensure complete drying. Since the hexagonal array was used in this study as an attempt to better represent the batch, *~edge* and *~central* T_i profiles were used separately to estimate the end of primary drying. **Table 1** displays these values and it can be observed that *~central* T_i estimated drying time was very close to Pi/Ba *offset* signal, being even slightly more conservative. This demonstrates the potential of this method as an alternative for end-time estimation.

(iv) Model parameters estimation using the IR camera

The temperature profile accuracy will reflect on K_v accuracy. For all tested vials, IR-based K_v values were comparable to thermocouple-based (**Figure A.12 A**, **C** and **E**) ones presenting

differences below 5% in most cases, although they did present higher differences for edge vials to up to 9.6% for 20R vials.

With an exploratory motivation, a map based on the IR temperature measurements was also generated. This map has one particularity: the first-row vials K_v is based on each individual vial temperature profile. This is a way to scrutinize the potentialities of the use of IR imaging. Since it is a non-invasive sensor and its use does not seem to significantly affect batch dynamics, it can be freely used to measure as many vials as intended - within the camera field of view. For the remaining edge vials, not in the first row, K_v was calculated based on the average ~*edge* IR profile while the central vials K_v was based on the average ~*central* IR profiles. This map is presented in **Figure 8** for 4R vials (and in **Figure A.13 A** and **A.13 B** respectively for 6R and 20R).

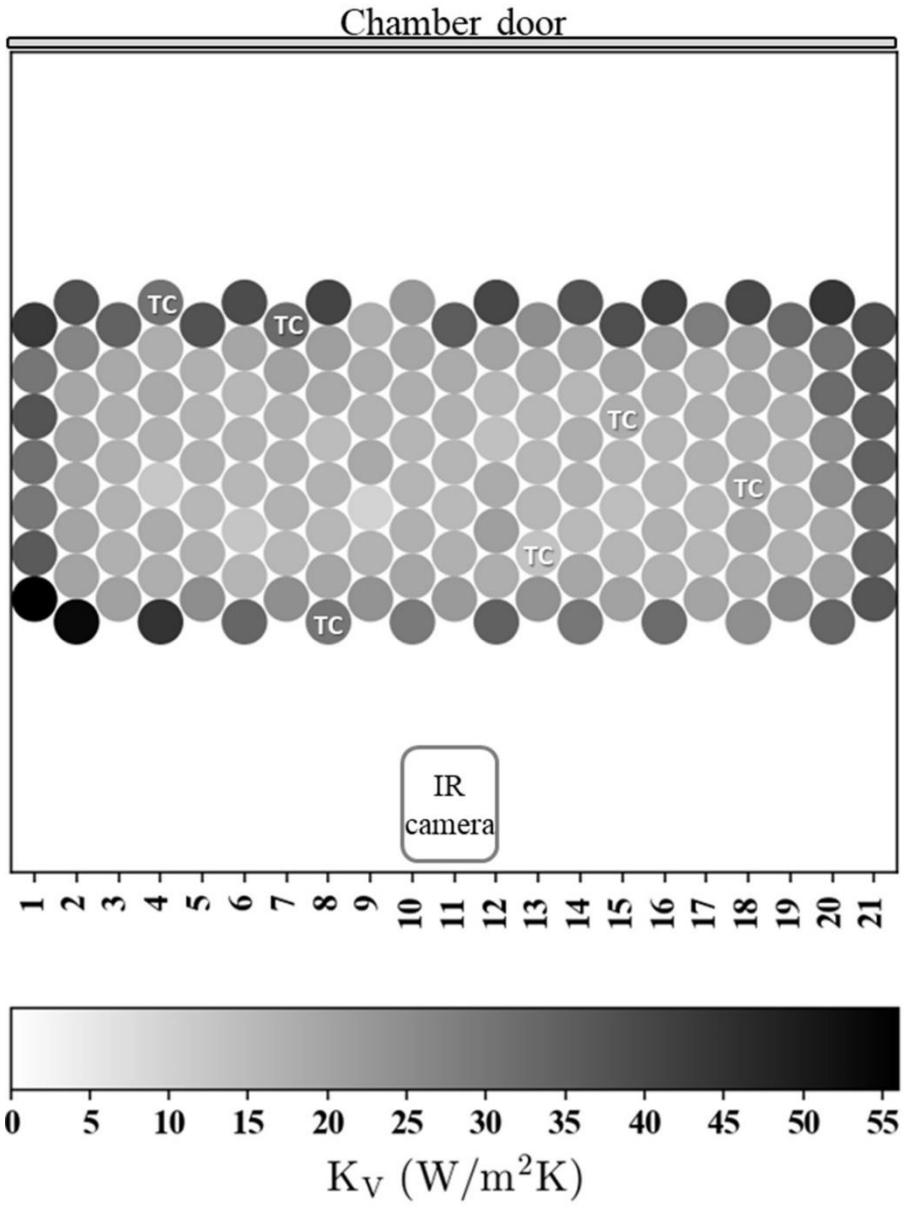

Figure 8. 4R vials K_v map using ~edge and ~central temperature values from the IR sensor. Additionally, each vial in the first row had its K_v calculated based on the individual IR temperature measurement.

It is worth noting how the use of individual vial measurements changed the heatmap pattern of the first row. Comparing it to **Figure 4 B** (K_v map of the same batch but based on thermocouple profiles), IR values rendered the vials further from the side walls a bit colder, with lower K_v values. Conversely, particularly for the leftmost vials, it rendered them warmer, with higher K_v values. This is of significant importance since it could be revealing a critical

control point during freeze-drying, as it was noted before that the left side seemed marginally warmer under the tested conditions. If it is known that those are the warmer vials in the batch, for a conservative process design, parameters based on these vials should be used. This would ensure no vial in the batch exceeds threshold temperature, such as the glass transition temperature when amorphous solutes are used or the eutectic point for crystalline ones.

Finally, R_p profiles based on each type of temperature measurement were analysed. This is a finer comparison as the calculations used are based on the ice vapor-pressure, which involves an exponential of the temperature measurements (**Equation (4)**), which may exacerbate even the smallest differences. Using the temperature data from the complete test, in which a 5% mannitol solution was used, the R_p profiles were calculated. Each resulting R_p curve was calculated based on the batch average temperature profile, from thermocouples or IR sensor measurements. Since this calculation is based on a simplified model, it is a good approximation in the beginning of drying. To address the whole cake profile, the R_p behavior is approximated through a curve fitting (**Equation (9)**). Both resulting R_p profiles (**Figure A.12 B**) are very close to each other and within range with values found in the literature for 5% sucrose [36]. Once again verifying the applicability of IR thermal profiles in freeze-drying. For 6R and 20R vials (**Figure A.12 D** and **F**), again, the R_p trend based on either temperature sensor resulted in comparable R_p profiles that can be successfully used for cycle design. The R_p values for mannitol 5% were also within the range found in the literature [26].

Conclusions

This study evaluated the effect and capabilities of the use of an IR sensor placed inside the chamber to monitor real-scale freeze-drying batches. From the starting points and objectives a few conclusions could be reached.

First, the sensor effect on larger batches from 30 to 157 vials is minimal and can be

neglected under the tested conditions. Regarding its accuracy, the measurements are typically within a ±2°C range with respect to thermocouples during primary drying. Furthermore, the IR sensor, as a non-invasive method, does not affect the product and removes the hassle of thermocouple proper placing for freeze drying batches. Additionally, with accurate temperature measurements throughout the process, the resulting variables for primary drying design space K_v and R_p, were estimated with good accuracy.

The hexagonal array approach worked in the tested conditions to provide an approximation of central vial behaviour. Additionally, it is necessary to stress the fact that, even though batches comprised up to 157 vials, they were conducted in a lab scale freeze dryer.

As for primary drying end time estimation, *~central* T_i estimated drying time provided a very adequate primary drying end time estimation when compared to the Pi/Ba method as they always fell within the *onset* and *offset* end-time range by this later method. *~central* T_i was capable of ensuring complete drying while providing a straightforward endpoint.

Edge vials' H profile could be accurately tracked using the IR sensor. However, this was limited to small cross section vials (4R and 6R) and the H end-times were always smaller than the K_v and the Pi/Ba ones. Moreover, they presented differences of up to 16.1% in end-time estimation compared to the K_v method and up to 18.4% compared to Pi/Ba onset values. This was still regarded as an accurate method for edge vials since when the Pi/Ba curve starts to decrease; these vials are most likely already dried. All methods have some inaccuracy, and it is impossible to determine an exact *true* value. The IR sensor presented could extract from its large array of thermal information different signals. These multiple simultaneous capabilities make it an all-in-one robust sensor.

Before concluding with the positive remarks of IR monitoring found in this study, it is important to point out its limitations. First, the sensor, in the present configuration, occupies a considerable amount of space inside the equipment. Which happens since it needs some

distance to the vials' frontline to have an adequate field of view. This can be minimized changing the focal point of the sensor and placing many small sensors to better represent the batch and monitor all sides. However, that should be tested in future studies. Another issue is that, although this sensor is designed in a food-grade case, it is not suitable for clean-in-place (CIP) processes. A solution to this can be making built-in systems in the future, coupled already with the freeze-drying equipment.

Nonetheless, the proposed IR sensor can reliably monitor a freeze-drying batch, while providing further insights into the process. The axial temperature profile allows the identification and tracking of the sublimation interface, which is a singular feature for this monitoring method. The non-invasive temperature monitoring, additionally, delivers a better product temperature profile and it can be properly used for freeze-drying design space determination.

The present study is a step forward towards the use of IR sensors to monitor industrial batches. Future studies should however include smaller sensors, possibly built-in and suitable to CIP processes to be adequate for industrial applications. Additionally, since industrial batch sizes can be very large, the hexagonal approach should also be further verified in such applications.

Acknowledgements

The contribution of Domenico Colucci in the first related studies with IR thermography and that of Daniela Ramirez in part of the experimental work is gratefully acknowledged by the authors.

List of References

[1] G. Reh, 2020 Global life sciences outlook, Deloitte Insights. (2020).
[2] A. Langford, B. Bhatnagar, R. Walters, S. Tchessalov, Drying technologies for biopharmaceutical applications: Recent developments and future direction, Dry. Technol. 36 (2018) 677–684. https://doi.org/10.1080/07373937.2017.1355318.

[3] M.B. Adali, A.A. Barresi, G. Boccardo, R. Pisano, Spray Freeze-Drying as a Solution to Continuous Manufacturing of Pharmaceutical Products in Bulk, Processes. 8 (2020) 21–27.
[4] S. Bosca, D. Fissore, Design and validation of an innovative soft-sensor for pharmaceuticals freeze-drying monitoring, Chem. Eng. Sci. 66 (2011) 5127–5136. https://doi.org/10.1016/j.ces.2011.07.008.
[5] D. Fissore, Freeze drying of pharmaceuticals, Encycl. Pharm. Sci. Technol. (2013) 37–41. https://doi.org/10.1081/E-EPT4-120050224.
[6] S.M. Patel, S. Chaudhuri, M.J. Pikal, Choked flow and importance of Mach I in freeze-drying process design, Chem. Eng. Sci. 65 (2010) 5716–5727. https://doi.org/10.1016/j.ces.2010.07.024.
[7] Food and Drug Administration, Guidance for Industry, PAT-A Framework for Innovative Pharmaceutical Development, Manufacturing and Quality Assurance, (2004). http://www.fda.gov/downloads/Drugs/GuidanceComplianceRegulatoryInformation/Guidances/ucm070305.pdf.
[8] D. Fissore, R. Pisano, A.A. Barresi, Process analytical technology for monitoring pharmaceuticals freeze-drying – a comprehensive review, Dry. Technol. 36 (2018) 1–27. https://doi.org/10.1080/07373937.2018.1440590.
[9] S.M. Patel, T. Doen, M.J. Pikal, Determination of end point of primary drying in freeze-drying process control, AAPS PharmSciTech. 11 (2010) 73–84. https://doi.org/10.1208/s12249-009-9362-7.
[10] T.R.M. De Beer, M. Wiggenhorn, R. Veillon, C. Debacq, Y. Mayeresse, B. Moreau, A. Burggraeve, T. Quinten, W. Friess, G. Winter, C. Vervaet, J.P. Remon, W.R.G. Baeyens, Importance of using complementary process analyzers for the process monitoring, analysis, and understanding of freeze drying, Anal. Chem. 81 (2009) 7639–7649. https://doi.org/10.1021/ac9010414.
[11] M. Demichela, A.A. Barresi, G. Baldissone, The Effect of Human Error on the Temperature Monitoring and Control of Freeze Drying Processes by Means of Thermocouples, Front. Chem. 6 (2018) 1–11. https://doi.org/10.3389/fchem.2018.00419.
[12] J.C. Kasper, M. Wiggenhorn, M. Resch, W. Friess, Implementation and evaluation of an optical fiber system as novel process monitoring tool during lyophilization, Eur. J. Pharm. Biopharm. 83 (2013) 449–459. https://doi.org/10.1016/j.ejpb.2012.10.009.
[13] S. Schneid, H. Gieseler, Evaluation of a new wireless temperature remote interrogation system (TEMPRIS) to measure product temperature during freeze drying, AAPS PharmSciTech. 9 (2008) 729–739. https://doi.org/10.1208/s12249-008-9099-8.
[14] I. Oddone, D. Fulginiti, A.A. Barresi, S. Grassini, R. Pisano, Non-Invasive Temperature Monitoring in Freeze Drying: Control of Freezing as a Case Study, Dry. Technol. 33 (2015) 1621–1630. https://doi.org/10.1080/07373937.2015.1040026.
[15] R. Pisano, D. Fissore, S.A. Velardi, A. Barresi, In-Line Optimization and Control of an Industrial Freeze-Drying Process for Pharmaceuticals, J. Pharm. Sci. 99 (2010) 4691–4709. https://doi.org/10.1002/jps.
[16] S. Bosca, A.A. Barresi, D. Fissore, Fast freeze-drying cycle design and optimization using a PAT based on the measurement of product temperature, Eur. J. Pharm. Biopharm. 85 (2013) 253–262. https://doi.org/10.1016/j.ejpb.2013.04.008.
[17] H. Emteborg, R. Zeleny, J. Charoud-Got, G. Martos, J. Lüddeke, H. Schellin, K. Teipel, Infrared thermography for monitoring of freeze-drying processes: Instrumental developments and preliminary results, J. Pharm. Sci. 103 (2014) 2088–2097. https://doi.org/10.1002/jps.24017.

[18] P.J. Van Bockstal, J. Corver, L. De Meyer, C. Vervaet, T. De Beer, Thermal Imaging as a Noncontact Inline Process Analytical Tool for Product Temperature Monitoring during Continuous Freeze-Drying of Unit Doses, Anal. Chem. 90 (2018) 13591–13599. https://doi.org/10.1021/acs.analchem.8b03788.
[19] E. Lietta, D. Colucci, G. Distefano, D. Fissore, On the use of infrared thermography for monitoring a vial freeze-drying process, J. Pharm. Sci. 108 (2018) 391–398. https://doi.org/10.1016/j.xphs.2018.07.025.
[20] R. Pisano, Automatic control of a freeze-drying process: Detection of the end point of primary drying, Dry. Technol. (2020) 1–18. https://doi.org/10.1080/07373937.2020.1774891.
[21] D. Colucci, R. Maniaci, D. Fissore, Monitoring of the freezing stage in a freeze-drying process using IR thermography, Int. J. Pharm. 566 (2019) 488–499. https://doi.org/10.1016/j.ijpharm.2019.06.005.
[22] M. Vollmer, K.-P. Möllmann, Infrared Thermal Imaging. Fundamentals, Research and Applications, 2nd ed., Wiley-VCH, Weinheim, Germany, 2006.
[23] ISO 18434-1, Conditions of monitoring and diagnostics of machines - Thermography, 03/01 (2008). https://doi.org/10.5594/J09750.
[24] D. Colucci, Infrared Imaging: a New Process Analytical Technology for Real Time Monitoring and Control of a Freeze-Drying Process, Politecnico di Torino, 2019.
[25] E. Sritham, S. Gunasekaran, Thermal evaluation of sucrose-maltodextrin-sodium citrate bioglass: Glass transition temperature, Food Hydrocoll. 60 (2016) 589–597. https://doi.org/10.1016/j.foodhyd.2016.04.030.
[26] D. Fissore, R. Pisano, A.A. Barresi, Using mathematical modeling and prior knowledge for QbD in freeze-drying processes, Springer Science, New York, 2015. https://doi.org/10.1007/978-1-4939-2316-8.
[27] S.A. Velardi, A.A. Barresi, Development of simplified models for the freeze-drying process and investigation of the optimal operating conditions, Chem. Eng. Res. Des. 86 (2008) 9–22. https://doi.org/10.1016/j.cherd.2007.10.007.
[28] M. Carfagna, M. Rosa, M. Lucke, A. Hawe, W. Frieß, Heat flux sensor to create a design space for freeze-drying development, Eur. J. Pharm. Biopharm. 153 (2020) 84–94. https://doi.org/10.1016/j.ejpb.2020.05.028.
[29] B. Scutellà, S. Passot, E. Bourlés, F. Fonseca, I.C. Tréléa, How Vial Geometry Variability Influences Heat Transfer and Product Temperature During Freeze-Drying, J. Pharm. Sci. 106 (2017) 770–778. https://doi.org/10.1016/j.xphs.2016.11.007.
[30] D. Fissore, M. Harguindeguy, D.V. Ramirez, T.N. Thompson, Development of freeze-drying cycles for pharmaceutical products using a micro freeze-dryer, J. Pharm. Sci. 109 (2019) 797–806. https://doi.org/10.1016/j.xphs.2019.10.053.
[31] K.H. Gan, R. Bruttini, O.K. Crosser, A.I. Liapis, Heating policies during the primary and secondary drying stages of the lyophilization process in vials: Effects of the arrangement of vials in clusters of square and hexagonal arrays on trays, Dry. Technol. 22 (2004) 1539–1575. https://doi.org/10.1081/DRT-200025596.
[32] D. Aydin, M. Memmedli, R.E. Omay, Smoothing Parameter Selection for Nonparametric Regression Using Smoothing Spline, Eur. J. Pure Appl. Math. 6 (2013) 222–238. www.ejpam.com.
[33] Gerald Farin, Curves and Surfaces for CAGD: A Practical Guide, 5th ed., Morgan Kaufmann Publishers AN, San Francisco, 2002. https://doi.org/10.1017/CBO9781107415324.004.
[34] A. Maity, M. Sherman, The two-sample t test with one variance unknown, Am. Stat. 60 (2006) 163–166. https://doi.org/10.1198/000313006X108567.
[35] E.A. Boss, R.M. Filho, E.C. Vasco De Toledo, Freeze drying process: Real time model

and optimization, Chem. Eng. Process. Process Intensif. 43 (2004) 1475–1485. https://doi.org/10.1016/j.cep.2004.01.005.
[36] B. Scutellà, I.C. Trelea, E. Bourlès, F. Fonseca, S. Passot, Determination of the dried product resistance variability and its influence on the product temperature in pharmaceutical freeze-drying, Eur. J. Pharm. Biopharm. 128 (2018) 379–388. https://doi.org/10.1016/j.ejpb.2018.05.004.

Temperature/end point monitoring and modelling of a batch freeze-drying process using an infrared camera

(Appendix A)

For the sake of brevity, all graphical results for 6R and 20R vials and some of the 4R ones were omitted from the main paper, although they were included in the discussion. In this Appendix, these results will be presented ahead. No further explanations will be given here as they were already examined throughout the paper.

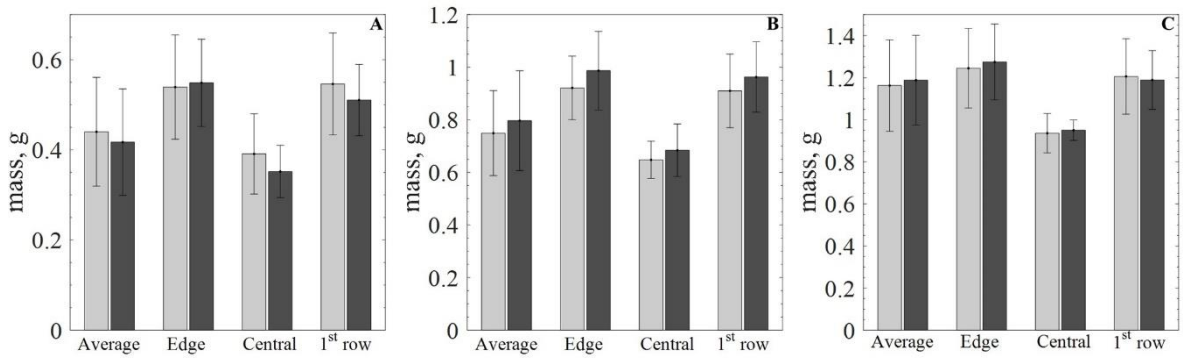

Figure A.1. Mass change after gravimetric test. Light grey bars represent the test done without the IR sensor; dark grey bars represent the test done with the IR sensor. **(A)** Shows results for 4R, **(B)** for 6R and **(C)** for 20R vials. Error bars indicate one standard deviation.

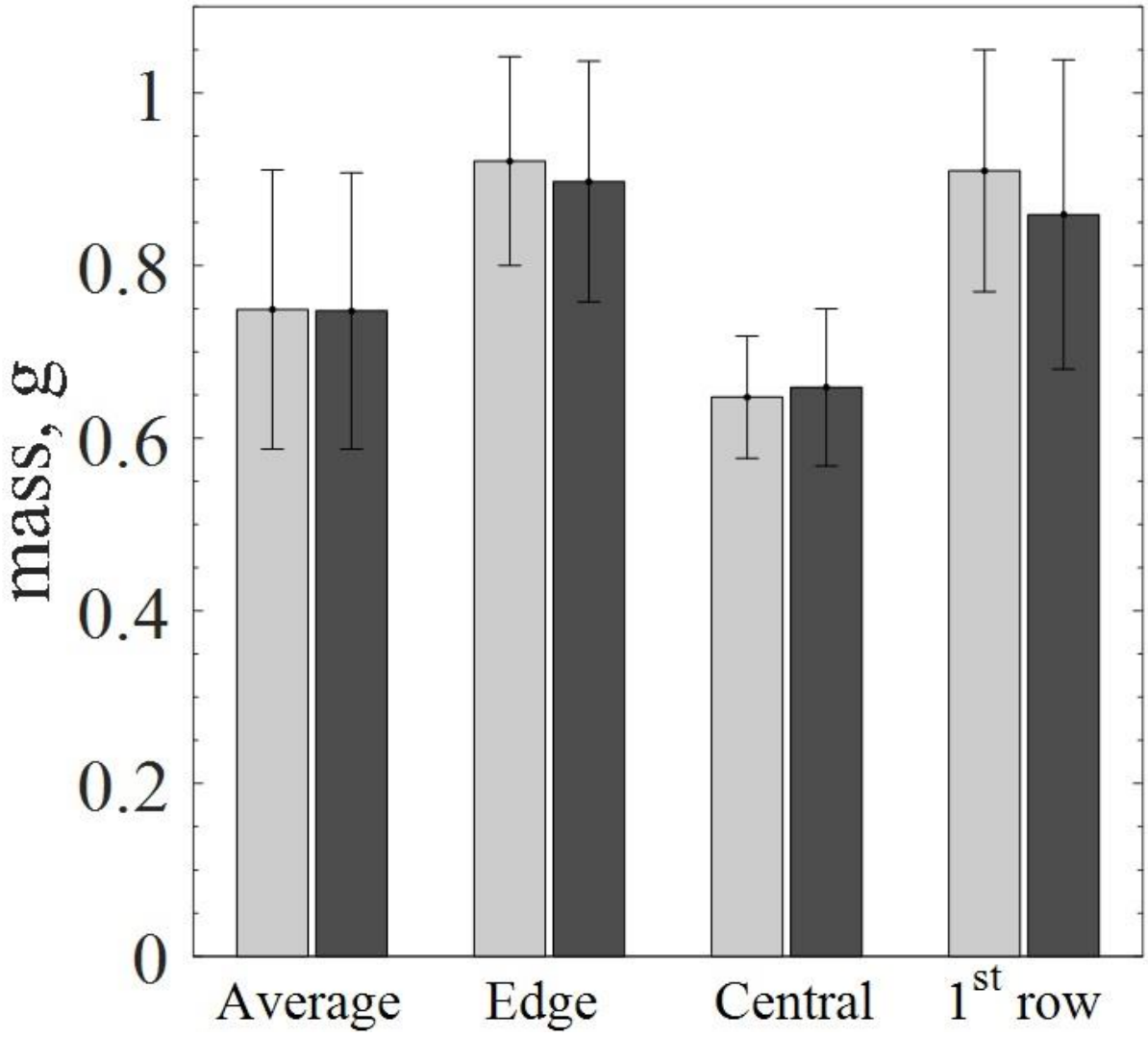

Figure A.2. Mass change after gravimetric test with long freezing for 6R vials. Light grey bars indicate test done without the IR sensor; dark grey bars indicate test done with the IR sensor. Error bars indicate one standard deviation.

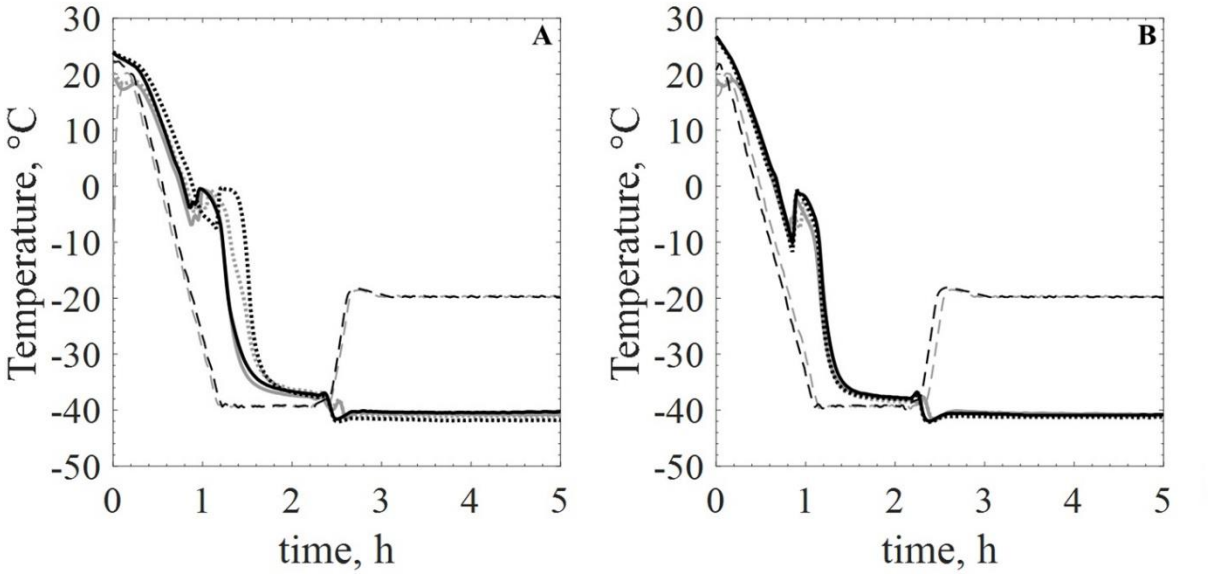

Figure A.3. Temperature profiles during gravimetric tests. Gray lines represent the test without the IR sensor while black lines represent the test with the IR sensor. Continuous lines (-) represent edge vials, dotted lines (.) represent central vials while dashed lines (- -) represent the shelf temperature throughout the test. **(A)** Shows results for 6R and **(B)** for 20R vials.

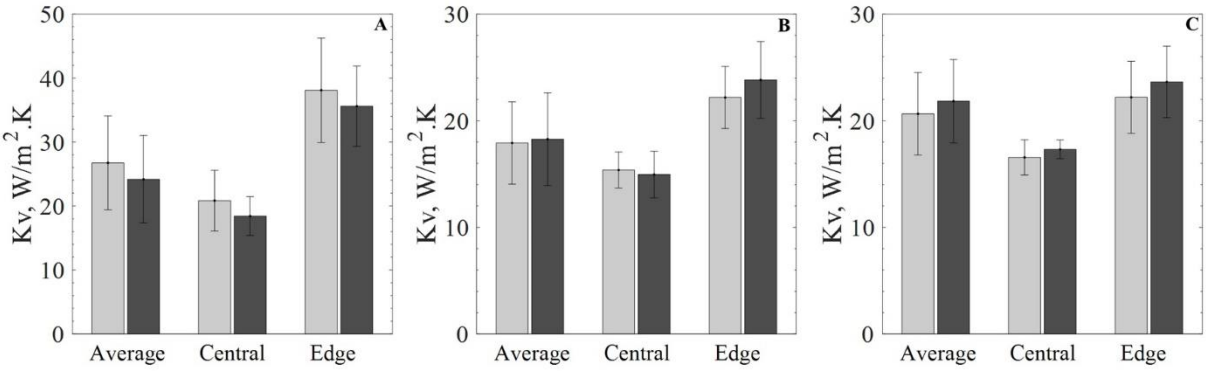

Figure A.4. Mean K_v values. Light grey bars indicate test done without the IR sensor; dark grey bars indicate test done with the IR sensor. **(A)** Shows results for 4R, **(B)** for 6R and **(C)** for 20R vials. Error bars indicate one standard deviation.

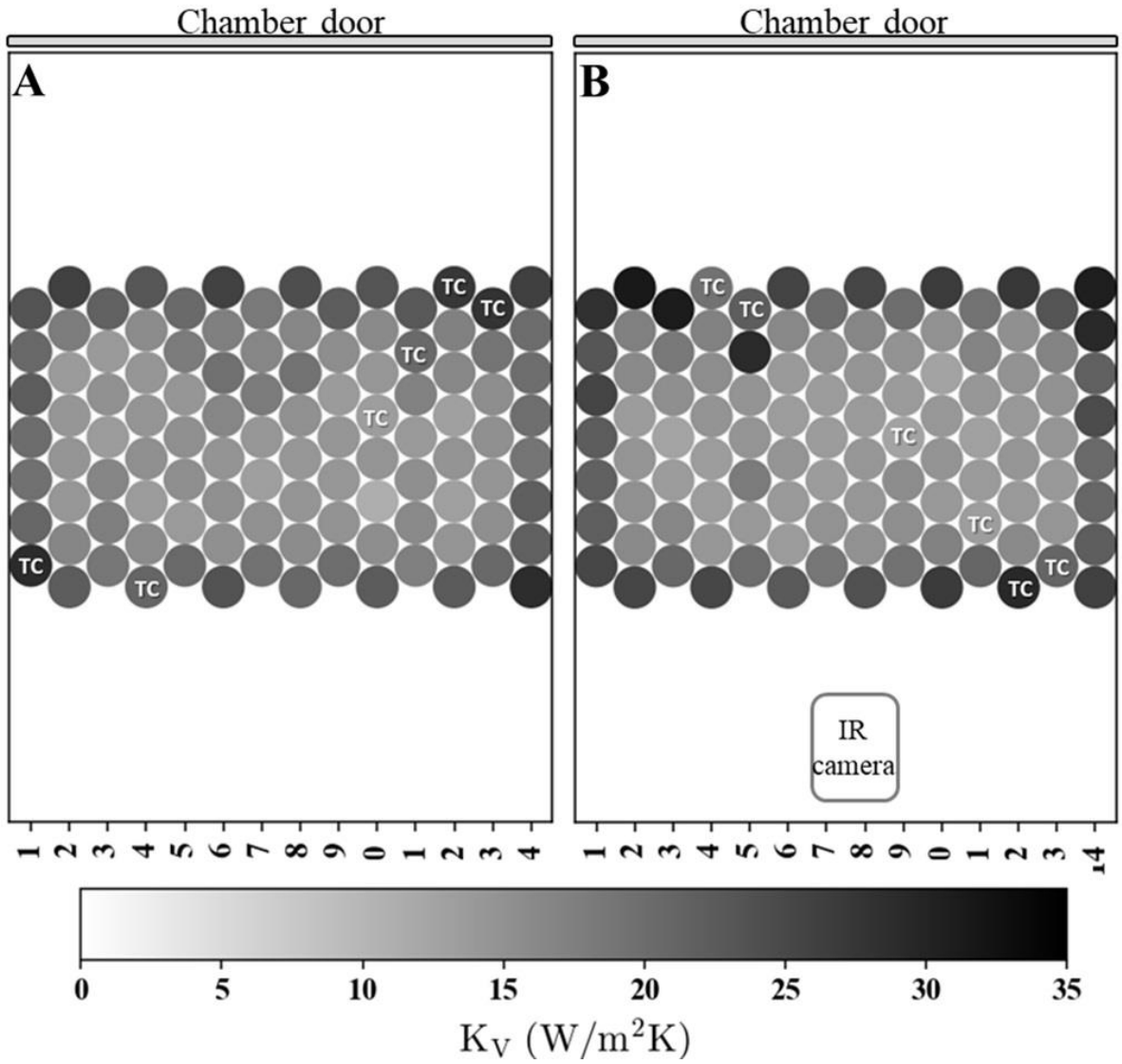

Figure A.5. K_v heat map for 6R vials. **(A)** Batch without the IR sensor inside the chamber; **(B)** batch with the IR sensor inside the chamber.

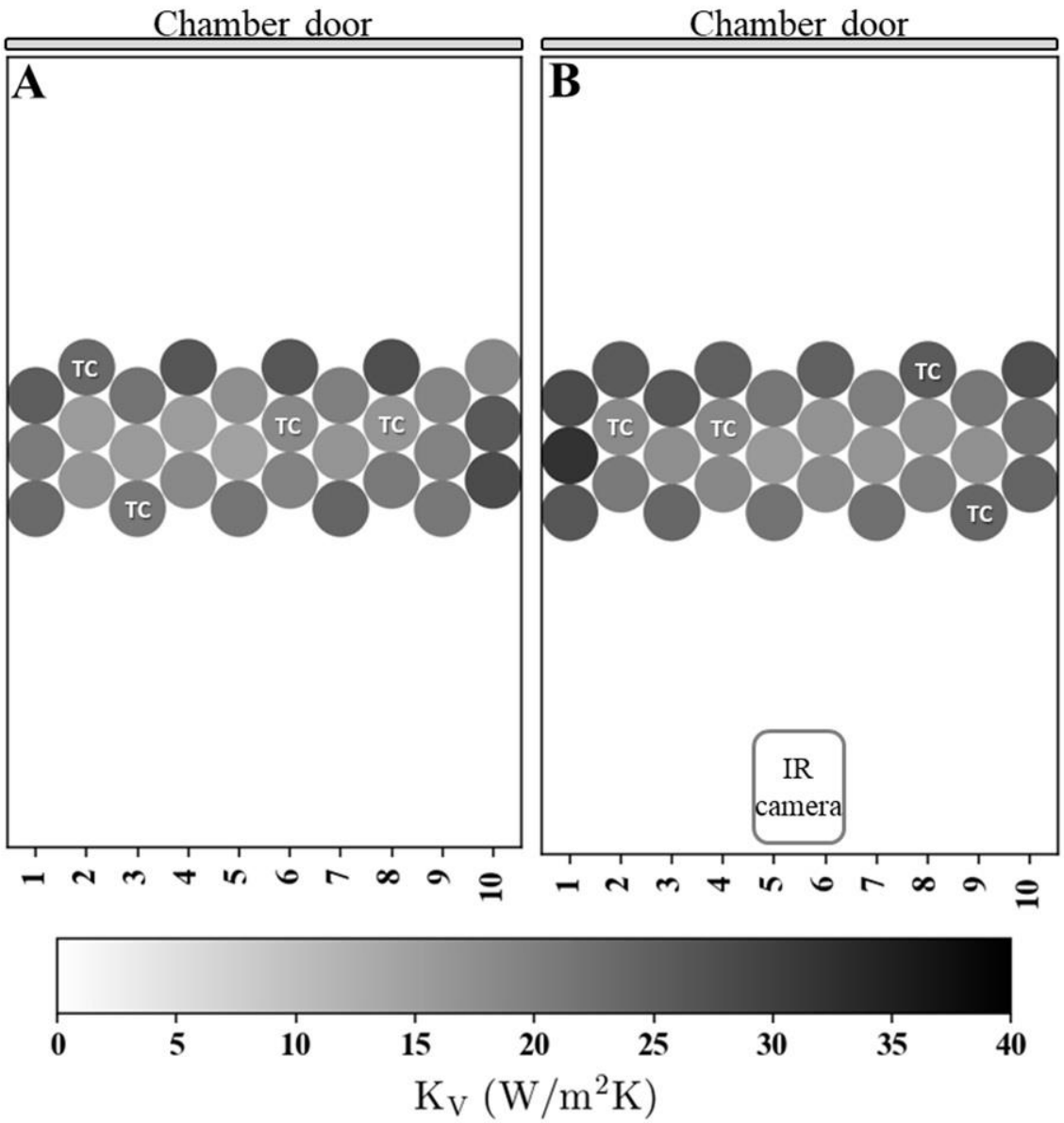

Figure A.6. K_v heat map for 20R vials. **(A)** Batch without the IR sensor inside the chamber; **(B)** batch with the IR sensor inside the chamber.

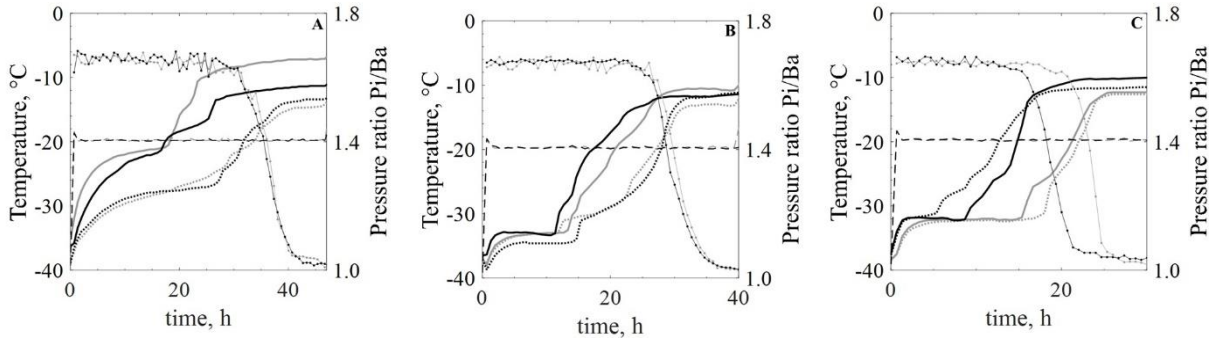

Figure A.7. Primary drying monitored profiles. Gray lines represent the test without the IR sensor while black lines represent the test with the IR sensor. Continuous lines (-) represent edge vials, dotted lines (.) represent central vials while dashed lines (- -) represent the shelf temperature throughout the test. The dot-dashed lines (.-) represent the Pirani/Baratron pressure ratio signals; **(A)** Shows results for 4R, **(B)** for 6R and **(C)** for 20R vials

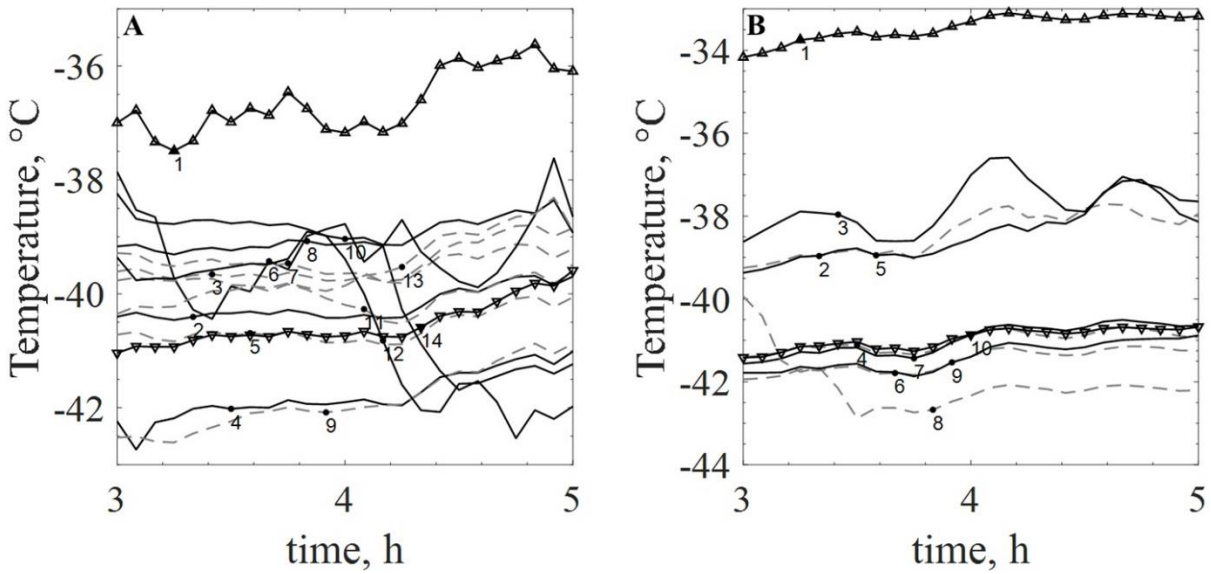

Figure A.8. IR bottom temperature profile by vial, in order from left to right, according to the thermal camera field of view The first (leftmost) vial is represented with a line and triangle (-▲), the last (rightmost) vial is represented by a line and inverted triangle (-▼). For all other vials, dashed lines represent *~central* vials while continuous lines represent *~edge* vials. **(A)** Shows results for 6R and **(B)** for 20R vials. Graph zoomed for the last 2 hours of primary drying.

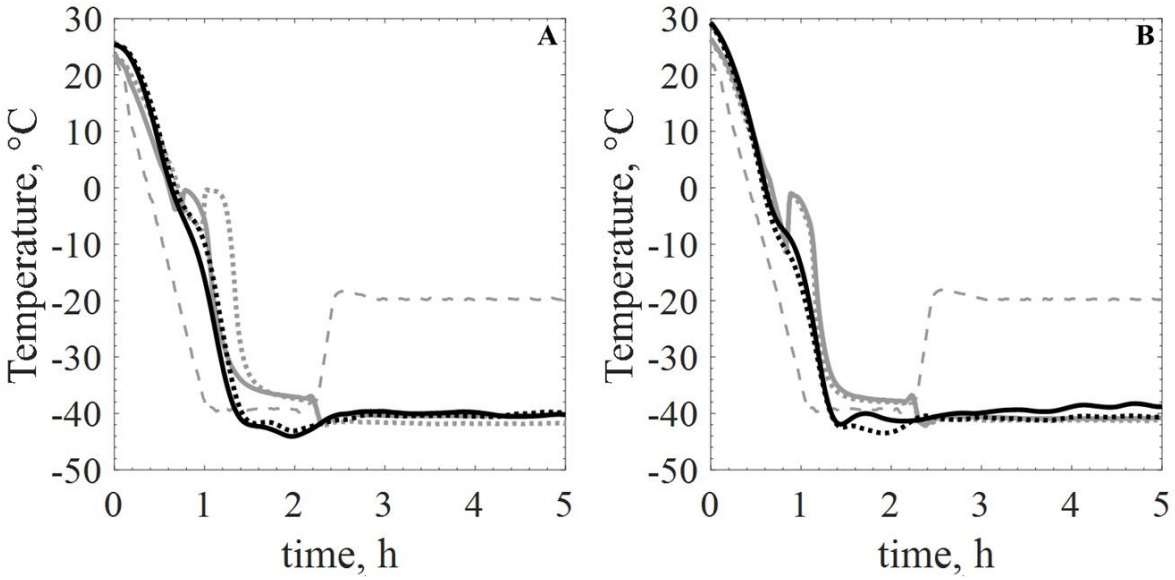

Figure A.9. TC versus IR average bottom temperature profiles for the same 4R vial batch. Continuous black line (-), IR ~*edge* vials. Dotted black line (.), IR ~*central* vials. Continuous grey line (-), TC edge vials. Dotted grey line (.), TC central vials. Dashed grey line (- -), shelf temperature. **(A)** Shows results for 6R and **(B)** for 20R vials.

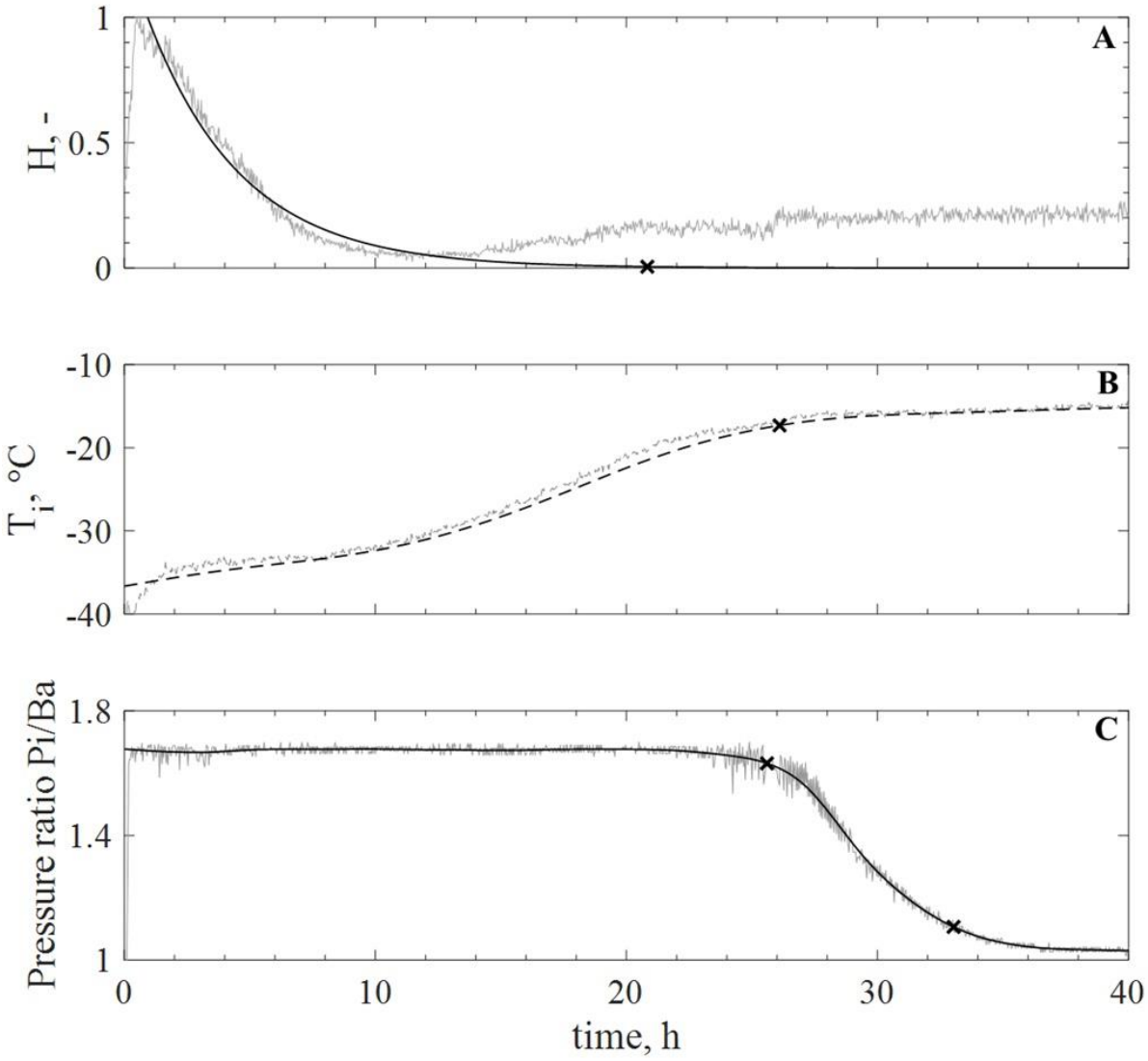

Figure A.10. Different signals to identify primary end-time for 6R vials. The "x" markers indicate potential end-time points for primary drying for each signal. In A, B and C, black line is the fitted smoothed curve while the grey line represents the raw data points. **(A)** Adimensional H axial profile where 1 represents the top of the vial and 0 the bottom, **(B)** Ti average profile, (C) $PiBa$ profile.

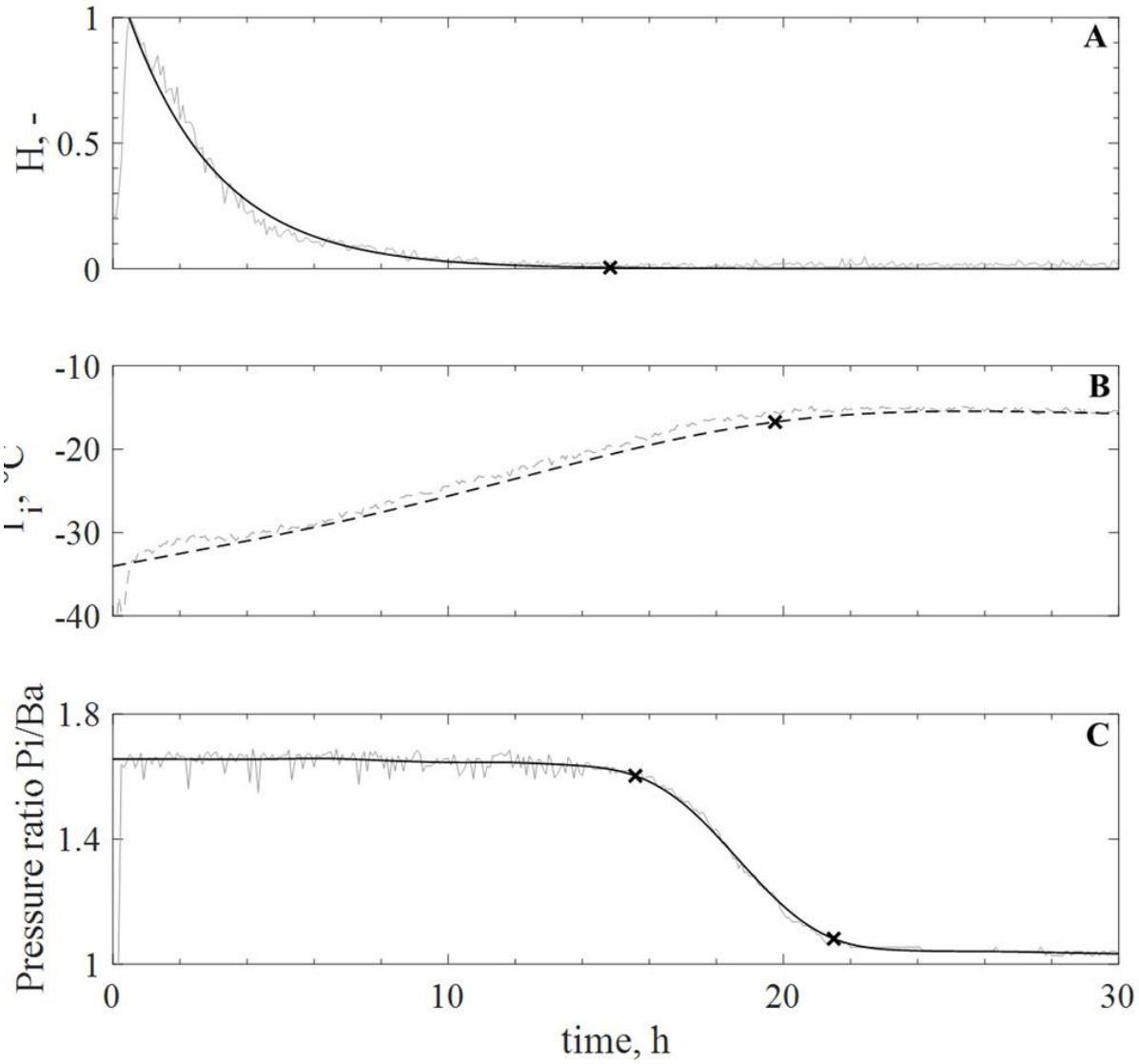

Figure A.11. Different signals to identify primary end-time for 20R vials. The "x" markers indicate potential end-time points for primary drying for each signal. In A, B and C, black line is the fitted smoothed curve while the grey line represents the raw data points. **(A)** Adimensional H axial profile where 1 represents the top of the vial and 0 the bottom, **(B)** Ti average profile, (C) Pi/Ba profile.

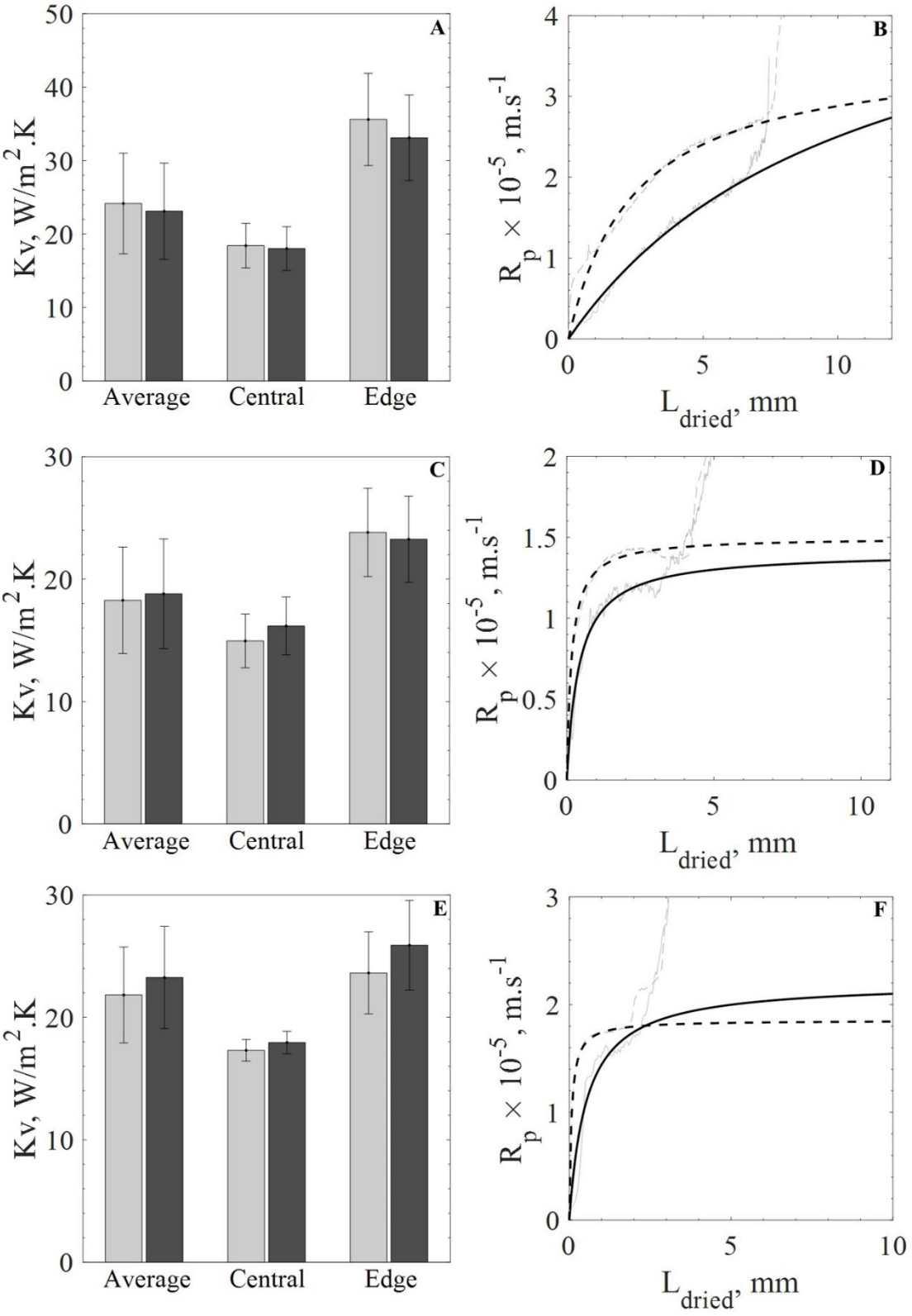

Figure A.12. Model parameters. K_v values for 4R **(A)**, 6R **(C)** and 20R **(E)**. The light grey bars indicate K_v based on thermocouple measurements and the dark grey bars indicate K_v based on IR temperature measurements. Error bars indicate one standard deviation. Then, R_p profiles for 4R **(B)**, 6R **(D)** and 20R **(F)**. The dashed (- -) lines represent R_p based on thermocouple temperature measurement while the continuous lines (-) represent R_p based on IR temperature measurements. The black lines represent the fitted R_p curves. The light grey lines show the raw data.

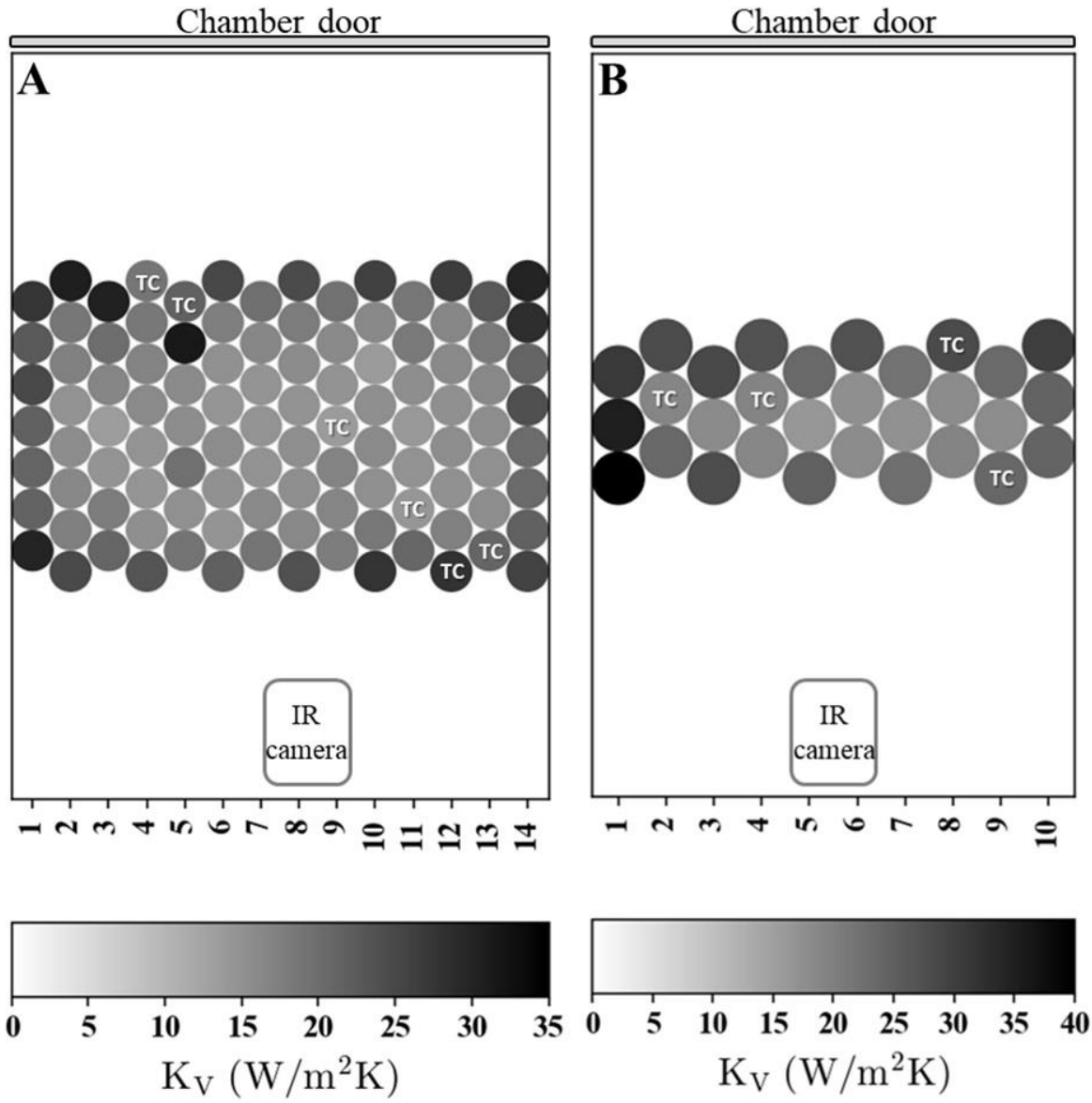

Figure A.13. K_v map using edge and central temperature values from the IR sensor. Additionally, each vial in the first row had its K_v calculated based on the individual IR temperature measurement. **(A)** Shows results for 6R and **(B)** for 20R vials.